

FlavBit: A GAMBIT module for computing flavour observables and likelihoods

The GAMBIT Flavour Workgroup: Florian U. Bernlochner¹, Marcin Chrz

- ¹Physikalisches Institut der Rheinischen Friedrich-Wilhelms-Universität Bonn, 53115 Bonn, Germany
²Physik-Institut, Universität Zürich, Winterthurerstrasse 190, 8057 Zürich, Switzerland
³H. Niewodniczański Institute of Nuclear Physics, Polish Academy of Sciences, 31-342 Kraków, Poland
⁴Department of Physics, University of Oslo, N-0316 Oslo, Norway
⁵Oskar Klein Centre for Cosmoparticle Physics, AlbaNova University Centre, SE-10691 Stockholm, Sweden
⁶Department of Physics, Stockholm University, SE-10691 Stockholm, Sweden
⁷Department of Physics, University of Adelaide, Adelaide, SA 5005, Australia
⁸Australian Research Council Centre of Excellence for Particle Physics at the Tera-scale
⁹NORDITA, Roslagstullsbacken 23, SE-10691 Stockholm, Sweden
¹⁰Univ Lyon, Univ Lyon 1, ENS de Lyon, CNRS, Centre de Recherche Astrophysique de Lyon UMR5574, F-69230 Saint-Genis-Laval, France
¹¹Theoretical Physics Department, CERN, CH-1211 Geneva 23, Switzerland
¹²LAPTh, Université de Savoie, CNRS, 9 chemin de Bellevue B.P.110, F-74941 Annecy-le-Vieux, France
¹³Department of Physics, Harvard University, Cambridge, MA 02138, USA
¹⁴Department of Physics, Imperial College London, Blackett Laboratory, Prince Consort Road, London SW7 2AZ, UK
¹⁵GRAPPA, Institute of Physics, University of Amsterdam, Science Park 904, 1098 XH Amsterdam, Netherlands

Received: date / Accepted: date

Abstract Flavour physics observables are excellent probes of new physics up to very high energy scales. Here we present FlavBit, the dedicated flavour physics module of the global-fitting package GAMBIT. FlavBit includes custom implementations of various likelihood routines for a wide range of flavour observables, including detailed uncertainties and correlations associated with LHCb measurements of rare, leptonic and semileptonic decays of B and D mesons, kaons and pions. It provides a generalised interface to external theory codes such as SuperIso, allowing users to calculate flavour observables in and beyond the Standard Model, and then test them in detail against all relevant experimental data. We describe FlavBit and its constituent physics in some detail, then give examples from supersymmetry and effective field theory illustrating how it can be used both as a standalone library for flavour physics, and within GAMBIT.

Contents

1	Introduction	1
2	Theoretical framework	2
3	Computational framework	3
4	Observables	3
4.1	Interfaces to external codes	4
4.2	Tree-level leptonic and semi-leptonic decays	4
4.3	Electroweak penguin transitions	6
4.4	Rare purely leptonic decays	10
4.5	Other flavour observables	10
5	Likelihoods	11
5.1	Tree-level leptonic and semi-leptonic likelihood	13
5.2	Electroweak penguin likelihood	14
5.3	Rare purely leptonic likelihood	15
5.4	Rare radiative B decay likelihood	15
5.5	B meson mass asymmetry likelihood	15
5.6	Other observables	15
6	Examples	15
6.1	Supersymmetric scan	16
6.2	Wilson coefficient fit	18
6.3	FlavBit standalone example	18
7	Conclusions	18
A	Glossary	19

^amchrzasz@cern.ch

^bnazila@cern.ch

^cp.scott@imperial.ac.uk

^dnicola.serra@cern.ch

*Also Institut Universitaire de France, 103 boulevard Saint-Michel, 75005 Paris, France.

1 Introduction

Precise measurement of flavour observables is a powerful indirect probe of physics beyond the Standard

Model (SM), as new heavy particles predicted by extensions of the SM can contribute to the amplitudes of observables as virtual particles. Flavour observables are therefore sensitive to much higher energy scales than direct searches for new particles. Moreover, rare decays, such as Flavour Changing Neutral Currents (FCNCs), are loop suppressed in the SM. As a consequence, the SM decay rates are small, and could be comparable in magnitude to contributions from new heavy states, allowing stringent constraints to be placed on the parameters of theories for new physics. It is therefore crucial to consider constraints from flavour physics when studying scenarios beyond the SM. The correlations between the different flavour observables, and the interplay between flavour measurements and direct searches at collider experiments, are key tools in the search for new physics, and its eventual understanding.

Public packages exist for carrying out SM and BSM flavour fits in terms of Wilson coefficients [1–3], but so far no general package exists for both computing Wilson coefficients and carrying out a global fit. In this article we present `FlavBit`, a flavour physics library designed in the context of the Global And Modular BSM Inference Tool (GAMBIT) framework [4], but also usable in standalone form. `FlavBit` allows users to predict flavour physics observables in various models, using external programs such as `SuperIso` [5–7], and then calculate combined likelihoods for arbitrary combinations of the observables. `FlavBit` takes into account all theoretical and experimental correlations between the different observables. The resulting likelihoods can be incorporated into the GAMBIT global likelihood to scan the parameter spaces of various models for new physics [4, 8–11], taking into account complementary constraints from direct production [12], dark matter searches [13], and SM and related precision measurements [14].

Recently, some measurements of flavour observables, mainly from LHCb [15–18] and B factories [19–23], have shown tension with their predicted values in the SM. It is still unclear if these might be accommodated in the SM by larger-than-expected QCD effects, statistical fluctuations or some combination thereof. Nonetheless, these tensions certainly provide motivation for continued interest and effort in careful combination and cross-correlation of flavour observables with each other, and with searches for new physics in other sectors. We include these measurements in `FlavBit`.

This paper is organised as follows. In Sec. 2 we provide the general theoretical background of the scheme by which we compute flavour observables, before providing a brief synopsis in Sec. 3 of the broader global-fitting framework within which `FlavBit` sits. In Sec. 4 we discuss the predictions and measurements of individual observ-

ables included in `FlavBit` 1.0.0, and highlight aspects of new physics models to which the different measurements are sensitive. Sec. 5 gives details of the likelihood calculations that `FlavBit` performs. Sec. 6 gives some usage examples, both in standalone mode and with GAMBIT proper. Sec. 7 summarises our conclusions, and Appendix A gives a glossary of relevant GAMBIT terminology helpful for reading this paper.

The `FlavBit` source code is freely available from gambit.hepforge.org under the terms of the standard 3-clause BSD license.¹

2 Theoretical framework

Our theoretical framework for studying rare decay observables is based on the effective Hamiltonian approach, which provides a simple formulation that can be easily extended to incorporate contributions from new physics. In this formulation, the low- and high-energy effects are separated using the Operator Product Expansion method. Cross-sections for transitions from initial states i to final states f are proportional to squared matrix elements $|\langle f | \mathcal{H}_{\text{eff}} | i \rangle|^2$, where the effective Hamiltonian \mathcal{H}_{eff} for $b \rightarrow s$ transitions is given by

$$\mathcal{H}_{\text{eff}} = -\frac{4G_F}{\sqrt{2}} V_{tb} V_{ts}^* \sum_{i=1}^{10} \left(C_i(\mu) \mathcal{O}_i(\mu) + C'_i(\mu) \mathcal{O}'_i(\mu) \right). \quad (1)$$

Here G_F is the Fermi constant, μ is the energy scale at which calculations are to be performed, and V_{tb} and V_{ts} are the usual CKM matrix elements. The C_i are Wilson coefficients, which incorporate the influence of small-scale physics due to heavy states that have been integrated out in the effective theory; their values can be calculated using perturbative methods. The \mathcal{O}_i are local operators representing long-distance interactions. The most relevant operators for the FCNC rare B decays are

$$\begin{aligned} \mathcal{O}_1 &= (\bar{s} \gamma_\mu T^a P_L c) (\bar{c} \gamma^\mu T^a P_L b), \\ \mathcal{O}_2 &= (\bar{s} \gamma_\mu P_L c) (\bar{c} \gamma^\mu P_L b), \\ \mathcal{O}_3 &= (\bar{s} \gamma_\mu P_L b) \sum_q (\bar{q} \gamma^\mu q), \\ \mathcal{O}_4 &= (\bar{s} \gamma_\mu T^a P_L b) \sum_q (\bar{q} \gamma^\mu T^a q), \end{aligned}$$

¹<http://opensource.org/licenses/BSD-3-Clause>. Note that `fjcore` [24] and some outputs of `FlexibleSUSY` [25] (incorporating routines from `SOFTSUSY` [26]) are also shipped with GAMBIT 1.0. These code snippets are distributed under the GNU General Public License (GPL; <http://opensource.org/licenses/GPL-3.0>), with the special exception, granted to GAMBIT by the authors, that they do not require the rest of GAMBIT to inherit the GPL.

$$\begin{aligned}
\mathcal{O}_5 &= (\bar{s}\gamma_{\mu_1}\gamma_{\mu_2}\gamma_{\mu_3}P_L b) \sum_q (\bar{q}\gamma^{\mu_1}\gamma^{\mu_2}\gamma^{\mu_3}q), \\
\mathcal{O}_6 &= (\bar{s}\gamma_{\mu_1}\gamma_{\mu_2}\gamma_{\mu_3}T^a P_L b) \sum_q (\bar{q}\gamma^{\mu_1}\gamma^{\mu_2}\gamma^{\mu_3}T^a q), \\
\mathcal{O}_7 &= \frac{e}{(4\pi)^2} m_b (\bar{s}\sigma^{\mu\nu}P_R b) F_{\mu\nu}, \\
\mathcal{O}_8 &= \frac{g}{(4\pi)^2} m_b (\bar{s}\sigma^{\mu\nu}T^a P_R b) G_{\mu\nu}^a, \\
\mathcal{O}_9 &= \frac{e^2}{(4\pi)^2} (\bar{s}\gamma^\mu P_L b) (\bar{\ell}\gamma_\mu \ell), \\
\mathcal{O}_{10} &= \frac{e^2}{(4\pi)^2} (\bar{s}\gamma^\mu P_L b) (\bar{\ell}\gamma_\mu \gamma_5 \ell), \tag{2}
\end{aligned}$$

where the sums run over $q = u, d, s, c, b$, m_b denotes the b quark mass, T^a are the $SU(3)_c$ generators, $F_{\mu\nu}$ and $G_{\mu\nu}^a$ are the photon and gluon stress-energy tensors respectively, and g is the strong coupling. A similar set of operators can also be defined for $b \rightarrow d$ transitions.

This formalism can be easily extended to incorporate effects of new physics, through additional contributions to the Wilson coefficients or the introduction of additional long-distance operators. For instance, the primed versions of these operators are chirality-flipped compared to the non-primed ones, and are highly suppressed in the SM. The scalar (\mathcal{Q}_1) and pseudoscalar (\mathcal{Q}_2) operators

$$\mathcal{Q}_1 = \frac{e^2}{(4\pi)^2} (\bar{s}P_R b) (\bar{\ell}\ell), \tag{3}$$

$$\mathcal{Q}_2 = \frac{e^2}{(4\pi)^2} (\bar{s}P_R b) (\bar{\ell}\gamma_5 \ell), \tag{4}$$

are absent in the SM, but receive large contributions in many models with an extended Higgs sector.

The Wilson coefficients are calculated by requiring matching between the high-scale theory and the low-energy effective theory at the scale μ_W , which is of the order of the W mass. Using the renormalisation group equations of the effective theory, they are then evolved to the scale μ_b (of the order of the b quark mass), which is the relevant scale for B physics calculations.

In order to compute the matrix element $\langle f | \mathcal{H}_{\text{eff}} | i \rangle$, which describes the transition from the initial state $|i\rangle$ to the final state $|f\rangle$, in addition to the relevant Wilson coefficients C_i , we need to evaluate the hadronic matrix elements $\langle f | \mathcal{O}_i | i \rangle$, which are usually the main source of uncertainties. These elements lead to decay constants and form factors that must be computed with techniques from non-perturbative QCD.

3 Computational framework

The GAMBIT framework defines two sorts of functions that can be used to calculate physical observables or other quantities required for computing them:

module functions: functions written in C++ and contained within a GAMBIT **module**.

backend functions: external library functions provided by a **backend**, such as SuperIso or FeynHiggs.

For ease of reference, here we **highlight** and link specific GAMBIT terms to their entries in the glossary, found in Appendix A.

When writing GAMBIT module functions, the author assigns each a **capability**, which describes what the function can calculate. This may be an observable, e.g. a particular branching fraction for a given rare B decay, or a likelihood, e.g. the combined likelihood defined using a set of rare decays. Module functions can be declared to have **dependencies** on the results of other module functions, which they indicate by specifying the **capability** of the module function that must be used to fill the dependency. Dependencies may be filled by any function within GAMBIT that has the requisite capability, whether or not it is part of the same GAMBIT **module** as the dependent function. Module functions may also have **backend requirements**, which are satisfied by functions from **backend** libraries. For example, in FlavBit 1.0.0, SuperIso supplies many of the backend requirements of the module functions that calculate observables.

FlavBit notifies GAMBIT of its available module functions and their capabilities, dependencies and backend requirements. The user tells GAMBIT that they want to compute a given set of observables and likelihoods in a given scan, and the GAMBIT Core identifies the necessary module functions and runs its **dependency resolution** routines. These hook the module functions up to each other and run them in an order that ensures that all dependencies are computed before the functions that depend on them. Full details of this process can be found in the main GAMBIT paper [4].

In standalone mode, users can just call the module functions of FlavBit directly, providing any required dependencies and backend requirements manually.

4 Observables

In this section we discuss the observables included in FlavBit and their relevance for searches for new physics.

The most important observables are the rare decays $B \rightarrow X_s \gamma$, $B_s^0 \rightarrow \mu^+ \mu^-$ and $B^0 \rightarrow K^{*0} \mu^+ \mu^-$, as well as tree level decays such as $B^\pm \rightarrow \tau \nu_\tau$ and $B \rightarrow D^{(*)} \ell \nu_\ell$.²

²Here $D^{(*)}$, B^\pm and ℓ are shorthand notations. The first indicates that we are referring to both $B \rightarrow D \ell \nu_\ell$ and $B \rightarrow D^* \ell \nu_\ell$, but as distinct processes. The same is true of the second notation, which indicates that we are referring to both the original process and its CP conjugate, distinctly. In contrast, when referring to

Here we discuss the calculation of the different observables in four groups: tree-level leptonic and semi-leptonic decays (Sec. 4.2), electroweak penguin transitions (Sec. 4.3), rare purely leptonic decays (Sec. 4.4), and other flavour observables (Sec. 4.5). In these sections we outline the calculations required to predict each observable from theory; further details can be found in Ref. [6]. While for simplicity we present only the leading order expressions in this paper, in `FlavBit` itself we use the full calculations at the highest available accuracy.

The tree-level category includes B and D decays to leptons with an accompanying hadron and/or a neutrino in the final state. Observables in this category are the branching fractions for processes such as $B^\pm \rightarrow \tau\nu_\tau$, $B \rightarrow D^{(*)}\tau\nu_\tau$ and $B \rightarrow D^{(*)}\ell\nu_\ell$. The electroweak penguin category includes the rare decays $B \rightarrow M\ell^+\ell^-$ (with M another meson lighter than the B), in particular the angular observables of the decay $B^0 \rightarrow K^{*0}\mu^+\mu^-$. The rare fully-leptonic category includes B decays with only leptons in the final state, such as $B_{(s)}^0 \rightarrow \mu^+\mu^-$. The fourth and final category includes $b \rightarrow s$ transitions in the radiative decays $B \rightarrow X_s\gamma$, the mass difference between the heavy B_H and light B_L eigenstates of the B_s^0 system (ΔM_s), and decays of kaons and pions, in particular the leptonic decay ratio $\mathcal{B}(K^\pm \rightarrow \mu\nu_\mu)/\mathcal{B}(\pi^\pm \rightarrow \mu\nu_\mu)$. Note that `FlavBit` does not incorporate the anomalous magnetic moment of the muon, as this is dealt with in `PrecisionBit` [14].

4.1 Interfaces to external codes

Theoretical predictions of observables in `FlavBit` are predominantly obtained through interfaces to external codes. Some predictions of flavour observables are available from `FeynHiggs` [27], for the SM and minimal supersymmetric SM (MSSM).³ In `FlavBit` 1.0.0, most observable calculations refer to `SuperIso` 3.6 [5–7].

The interface to `SuperIso` operates via the function `SI_fill` (see Table 1), which provides the `SuperIso_modelinfo`. This function fills a `SuperIso_parameters` structure, which is passed back to various other `SuperIso` functions to compute observables. Observables that are calculated directly from the input model parameters (Table 1) are distinguished from those that involve the calculation of intermediate Wilson coeffi-

specific rates, ℓ is typically used to indicate that the final state does not distinguish between $\ell = e$ and $\ell = \mu$. Some groups use this notation to refer to a sum over all final states involving electrons and muons, others use it to refer to the average. The PDG uses the former notation, which we follow in this paper except where explicitly noted otherwise.

³The `GAMBIT` interface to `FeynHiggs` is described in detail in Sec 3.1.3 of Ref. [14].

icients (Tables 2 and 3). In `FlavBit` 1.0.0, observables are implemented for MSSM models (‘MSSM63atQ’ and descendants; see [4]), and for a flavour EFT model (‘WC’) where the Wilson coefficients are specified directly as model parameters, and scanned over.

The design of `FlavBit` and its interface to `SuperIso` make extending `FlavBit` to other models quite straightforward, either by computing Wilson coefficients ‘upstream’ from fundamental parameters, or by constructing the `SuperIso_modelinfo` to fit the model under investigation. `SI_fill` deals with the majority of the model-dependence in each calculation, importing different masses and couplings from `SpecBit` depending on the model being scanned, and using them to set various flags and member variables of the `SuperIso_modelinfo`.

`SI_fill` has a single option configurable from the master YAML file of a given scan: a boolean flag `take_b_pole_mass_from_spectrum`. This option allows the user to choose between `SuperIso`’s internal calculation of the b quark pole mass (based on the \overline{MS} mass imported from `GAMBIT`), or `GAMBIT`’s own b pole mass calculation provided by `SpecBit` [14]. Depending on the spectrum generator chosen in `SpecBit`, the standard 2-loop conversion from \overline{MS} to pole mass included in `SuperIso` may be a more accurate choice for precision B physics than other calculations, even if the other calculation includes higher-order corrections. This is because the b pole is sufficiently close to the QCD scale that problems with the perturbative expansion required to compute it start to show already at 3 loops [28], such that the formal error on the b pole mass associated with truncating the asymptotic series may already be larger when truncating at 3 rather than 2 loops. This means that although 3-loop QCD RGEs remain preferable, 2-loop self energies give a more precise value for the b pole, and should be preferred for B physics calculations. In `FlavBit` 1.0.0, `take_b_pole_mass_from_spectrum` therefore defaults to `false`.⁴

4.2 Tree-level leptonic and semi-leptonic decays

Decays of B mesons with leptons and neutrinos in the final state proceed via tree-level charged currents. They have been intensively studied at B factories (Babar, Belle and CLEO) for the determination of the elements V_{cb} and V_{ub} of the CKM matrix.

⁴Note that `SuperIso` only actually uses the b pole mass for computing the 1S mass, which is better-behaved than the pole mass and preferable for observable calculations.

Capability	Function (Return Type): Brief Description	Dependencies (Model)	Backend requirements
SuperIso_modelinfo	<code>SI_fill</code> (<code>parameters</code>): Fills the SuperIso structure. Key routine of the SuperIso interface.	<code>MSSM_spectrum</code> (MSSM63atQ) <code>SM_spectrum</code> (WC) <code>W_plus_decay_rates</code> <code>Z_decay_rates</code>	<code>Init_param</code> <code>slha_adjust</code> <code>mb_1S</code>
Dstaunu	<code>SI_Dstaunu</code> (<code>double</code>): Computes the branching fraction of $D_s^\pm \rightarrow \tau\nu_\tau$.	SuperIso_modelinfo	Dstaunu
Dsmunu	<code>SI_Dsmunu</code> (<code>double</code>): Computes the branching fraction of $D_s^\pm \rightarrow \mu\nu_\mu$.	SuperIso_modelinfo	Dsmunu
Dmunu	<code>SI_Dmunu</code> (<code>double</code>): Computes the branching fraction of $D^\pm \rightarrow \mu\nu_\mu$.	SuperIso_modelinfo	Dmunu
Btaunu	<code>SI_Btaunu</code> (<code>double</code>): Computes the branching fraction of $B^\pm \rightarrow \tau\nu_\tau$.	SuperIso_modelinfo	Btaunu
BDtaunu	<code>SI_BDtaunu</code> (<code>double</code>): Computes the branching fraction of $B \rightarrow D\tau\nu_\tau$.	SuperIso_modelinfo	BRBD1nu
BDmunu	<code>SI_BDmunu</code> (<code>double</code>): Computes the branching fraction of $B \rightarrow D\mu\nu_\mu$.	SuperIso_modelinfo	BRBD1nu
BDstartaunu	<code>SI_BDstartaunu</code> (<code>double</code>): Computes the branching fraction of $B \rightarrow D^*\tau\nu_\tau$.	SuperIso_modelinfo	BRBDstar1nu
BDstarmunu	<code>SI_BDstarmunu</code> (<code>double</code>): Computes the branching fraction of $B \rightarrow D^*\mu\nu_\mu$.	SuperIso_modelinfo	BRBDstar1nu
RD	<code>SI_RD</code> (<code>double</code>): Computes the ratio $\mathcal{B}(B \rightarrow D\tau\nu_\tau)/\mathcal{B}(B \rightarrow D\ell\nu_\ell)$, where $\ell = \mu$ or e and the result is the same for each.	SuperIso_modelinfo	BDtaunu_BDenu
RDstar	<code>SI_RDstar</code> (<code>double</code>): Computes the ratio $\mathcal{B}(B \rightarrow D^*\tau\nu_\tau)/\mathcal{B}(B \rightarrow D^*\ell\nu_\ell)$, where $\ell = \mu$ or e and the result is the same for each.	SuperIso_modelinfo	BDstartaunu_BDstarenu
Rmu	<code>SI_Rmu</code> (<code>double</code>): Computes the ratio $\mathcal{B}(K^\pm \rightarrow \mu\nu_\mu)/\mathcal{B}(\pi^\pm \rightarrow \mu\nu_\mu)$.	SuperIso_modelinfo	Kmunu_pimunu
Rmu23	<code>SI_Rmu23</code> (<code>double</code>): Computes the observable $R_{\mu 23}$ (Eq. 32).	SuperIso_modelinfo	Rmu23
FH_FlavourObs	<code>FH_FlavourObs</code> (<code>fh_FlavourObs</code>): Computes the FeynHiggs flavour observables.		FHFlavour
deltaMs	<code>FH_DeltaMs</code> (<code>double</code>): Extracts the FeynHiggs MSSM prediction for the $B_s - \bar{B}_s$ mass difference ΔM_s (in ps^{-1}).	FH_FlavourObs	

Table 1: Observable capabilities of FlavBit that do not involve Wilson coefficients. Details of the `fh_FlavourObs` structure can be found in Table 5.

The rate of the semi-leptonic decay $B \rightarrow M\ell\nu_\ell$ in the SM is

$$\frac{d\Gamma}{dq^2} = \frac{G_F^2 |V_{qb}|^2}{192\pi^3 m_B^3} \mathcal{K}(m_B^2, m_M^2, q^2) \mathcal{F}^{(2)}(q^2), \quad (5)$$

where $q^\mu = p_B^\mu - p_M^\mu$ is the momentum transfer, V_{qb} is the CKM element corresponding to the flavour of M , \mathcal{K} is a phase-space factor and $\mathcal{F}^{(2)}(q^2)$ is a combination of form factors [29].

These decays are sensitive to charged-current contributions from new particles. For example, the charged Higgs in the two Higgs doublet model (2HDM) (see e.g. Refs. [30–33]), right-handed currents via the contribution of the charged mediator W_R [32, 34], new left-handed heavy bosons W' [35, 36] and leptoquarks

(see e.g. Refs. [37, 38]) can also modify the value of this observable.

The decays $B^\pm \rightarrow \ell\nu_\ell$ also proceed via tree-level charged currents. The branching fraction is

$$\mathcal{B}(B^+ \rightarrow \ell^+\nu_\ell) = \frac{G_F^2 m_B m_\ell^2}{8\pi} \left(1 - \frac{m_\ell^2}{m_B^2}\right)^2 f_B^2 |V_{ub}|^2 \tau_B, \quad (6)$$

where f_B is the meson decay constant and τ_B is the lifetime of the B^+ . This decay is sensitive to the CKM element V_{ub} . The charged Higgs sector of the 2HDM can again provide substantial contributions, as can new charged gauge bosons like the W' and W_R of the left-right symmetric model [39]. Compared to the case where $\ell = \tau$, the decays with $\ell = e$ and $\ell = \mu$ have

much smaller branching fractions, as they are helicity-suppressed. For this reason, at present only upper limits are available for the decays to light leptons. Although we provide routines to predict the values of all three in **FlavBit**, we only incorporate the tauonic version into the resulting likelihood.

Similarly, the decays $D_{(s)}^\pm \rightarrow \ell \nu_\ell$ are mediated by the W boson in the SM. The branching fractions can be obtained from Eq. 6 after the replacement $B \rightarrow D_{(s)}$ and swapping in the relevant CKM element. These decays have been traditionally used to measure the $D_{(s)}$ meson decay constant. However, the charged Higgs boson in the 2HDM would also mediate these decays, so they can provide complementary constraints to the analogous B meson decay [40].

As shown in Table 1, **FlavBit** provides functions capable of computing branching fractions for $D_s^\pm \rightarrow \tau \nu_\tau$ (**Dstaunu**), $D_s^\pm \rightarrow \mu \nu_\mu$ (**Dsmunu**), $D^\pm \rightarrow \mu \nu_\mu$ (**Dmunu**), $B^\pm \rightarrow \tau \nu_\tau$ (**Btaunu**), $B \rightarrow D \tau \nu_\tau$ (**BDtaunu**), $B \rightarrow D \mu \nu_\mu$ (**BDmunu**), $B \rightarrow D^* \tau \nu_\tau$ (**BDstartaunu**) and $B \rightarrow D^* \mu \nu_\mu$ (**BDstarmunu**). It can also compute $R_{D^{(*)}} \equiv \mathcal{B}(B \rightarrow D^{(*)} \tau \nu_\tau) / \mathcal{B}(B \rightarrow D^{(*)} \ell \nu_\ell)$, designated by capabilities **RD** and **RDstar**. Here ℓ in $R_{D^{(*)}}$ refers to either μ or e , not their sum (the branching fractions $B \rightarrow D^{(*)} \ell \nu_\ell$ are identical for e and μ , as both are effectively massless in the B system).

4.3 Electroweak penguin transitions

Rare semi-leptonic decays of B mesons proceed via flavour-changing neutral currents (FCNCs) in electroweak penguin diagrams, and set stringent constraints on possible contributions from new physics. **FlavBit** includes predictions of various FCNC $b \rightarrow s$ transitions. These decays are all proportional to the elements V_{tb} and V_{ts} of the CKM matrix.

Rare decays of the type $B \rightarrow M \ell^+ \ell^-$, with one meson M in the final state, are sensitive to the Wilson coefficients $C_{9,10}^{(\prime)}$. In addition, when M is a vector, such as the $K^*(892)$, these decays are also sensitive to the Wilson coefficients $C_7^{(\prime)}$.

The four-quark operators ($\mathcal{O}_{1\dots 6}$) in the effective Hamiltonian also contribute to the penguin diagrams, resulting in expressions with the same structure as \mathcal{O}_7 and \mathcal{O}_9 . They can therefore be reabsorbed and used to define effective Wilson coefficients C_7^{eff} and C_9^{eff} [41],

$$C_7^{\text{eff}} = C_7 - \frac{1}{3}C_3 - \frac{4}{9}C_4 - \frac{20}{3}C_5 - \frac{80}{9}C_6, \quad (7)$$

$$C_9^{\text{eff}} = C_9 + Y(q^2), \quad (8)$$

where Y contains the short distance contributions from the four-quark operators [42, 43].

The most accessible of the $B \rightarrow M \ell^+ \ell^-$ decays at LHCb are those including final-state muons. The differential decay rate for $B \rightarrow M \mu^+ \mu^-$, where M is a pseudoscalar, is given at leading order by [44]:

$$\begin{aligned} \frac{d\Gamma}{dq^2} = & \frac{G_F^2 \alpha^2 |V_{tb} V_{ts}^*|^2 m_B^3}{(2\pi)^{10}} u(q^2) \left\{ v(q^2) |C_{10} f_+(q^2)|^2 \right. \\ & \left. + 4 \frac{m_\mu^2 (m_B^2 - m_M^2)^2}{q^2 m_B^4} |C_{10} f_0(q^2)|^2 \right. \\ & \left. + \left| C_9^{\text{eff}} f_+(q^2) + 2 \frac{m_b + m_s}{m_B + m_M} C_7^{\text{eff}} f_T(q^2) \right|^2 \right\}, \quad (9) \end{aligned}$$

where $u(q^2)$ and $v(q^2)$ are kinematic factors, and f_0 , f_+ and f_T are q^2 -dependent form factors.

If M is a vector particle, the $B \rightarrow M \ell^+ \ell^-$ decays are completely described by the dilepton invariant mass squared q^2 and three angles (θ_l, θ_K and ϕ ; see Ref. [45, 46] for definitions). Measurements of angular observables of the decays $B^0 \rightarrow K^*(892) \mu^+ \mu^-$ and $B_s^0 \rightarrow \phi \mu^+ \mu^-$ provide a better sensitivity to new physics than measurements of branching fractions. As a function of q^2 and the three angles, the differential decay rate for $B^0 \rightarrow K^{*0} \mu^+ \mu^-$ is

$$\begin{aligned} \frac{1}{\Gamma} \frac{d^3(\Gamma + \bar{\Gamma})}{d \cos \theta_\ell d \cos \theta_K d\phi} = & \frac{9}{32\pi} \left[\frac{3}{4} (1 - F_L) \sin^2 \theta_K \right. \\ & \left. + F_L \cos^2 \theta_K + \frac{1}{4} (1 - F_L) \sin^2 \theta_K \cos 2\theta_\ell \right. \\ & - F_L \cos^2 \theta_K \cos 2\theta_\ell + S_3 \sin^2 \theta_K \sin^2 \theta_\ell \cos 2\phi \\ & + S_4 \sin 2\theta_K \sin 2\theta_\ell \cos \phi + S_5 \sin 2\theta_K \sin \theta_\ell \cos \phi \\ & + \frac{4}{3} A_{\text{FB}} \sin^2 \theta_K \cos \theta_\ell + S_7 \sin 2\theta_K \sin \theta_\ell \sin \phi \\ & \left. + S_8 \sin 2\theta_K \sin 2\theta_\ell \sin \phi + S_9 \sin^2 \theta_K \sin^2 \theta_\ell \sin 2\phi \right], \quad (10) \end{aligned}$$

where $\bar{\Gamma}$ is the decay rate of the CP conjugate mode. The angular observable F_L is the longitudinal polarisation fraction of the K^* . The other observables are S_i , and the forward-backward asymmetry A_{FB} . The most sensitive experimental analyses assume that there are no scalar contributions (which are constrained by the branching fraction of $B_s^0 \rightarrow \mu^+ \mu^-$), and no tensor contributions.⁵ This assumption makes it possible to eliminate the observables S_1^c, S_1^s, S_2^c and S_2^s in favour of a single observable F_L . The physical observables are sesquilinear combinations of the transversity amplitudes [49],

$$F_L = 1 - F_T = \frac{A_0^2}{A_{\parallel}^2 + A_{\perp}^2 + A_0^2}, \quad (11)$$

⁵Although Ref. [47] includes measurements free from these assumptions, using the Method of Moments [48], the resulting precision is about 15% less than in the likelihood fit.

Capability	Function (Return Type): Brief Description	Dependencies	Backend requirements
bsgamma	<code>SI_bsgamma</code> (double): Computes the inclusive branching fraction of $B \rightarrow X_s \gamma$ for $E_\gamma > 1.6$ GeV.	<code>SuperIso_modelinfo</code>	<code>bsgamma_CONV</code>
	<code>FH_bsgamma</code> (double): Extracts the total inclusive branching fraction of $B \rightarrow X_s \gamma$ in the MSSM from <code>FeynHiggs</code> .	<code>FH_FlavourObs</code>	
delta0	<code>SI_delta0</code> (double): Computes the isospin asymmetry of $B \rightarrow K^* \gamma$.	<code>SuperIso_modelinfo</code>	<code>delta0_CONV</code>
Bsmumu_untag	<code>SI_Bsmumu_untag</code> (double): Computes the CP -averaged branching fraction of $B_s^0 \rightarrow \mu^+ \mu^-$.	<code>SuperIso_modelinfo</code>	<code>Bsll_untag_CONV</code>
	<code>FH_Bsmumu</code> (double): Extracts the CP -averaged branching fraction of $B_s^0 \rightarrow \mu^+ \mu^-$ in the MSSM from <code>FeynHiggs</code> .	<code>FH_FlavourObs</code>	
Bsee_untag	<code>SI_Bsee_untag</code> (double): Computes the CP -averaged branching fraction of $B_s^0 \rightarrow e^+ e^-$.	<code>SuperIso_modelinfo</code>	<code>Bsll_untag_CONV</code>
Bmumu	<code>SI_Bmumu</code> (double): Computes the branching fraction of $B^0 \rightarrow \mu^+ \mu^-$.	<code>SuperIso_modelinfo</code>	<code>Bll_CONV</code>
BRBXsmumu_lowq2	<code>SI_BRBXsmumu_lowq2</code> (double): Computes the inclusive low- q^2 branching fraction of $B \rightarrow X_s \mu^+ \mu^-$.	<code>SuperIso_modelinfo</code>	<code>BRBXsmumu_lowq2_CONV</code>
BRBXsmumu_highq2	<code>SI_BRBXsmumu_highq2</code> (double): Computes the inclusive high- q^2 branching fraction of $B \rightarrow X_s \mu^+ \mu^-$.	<code>SuperIso_modelinfo</code>	<code>BRBXsmumu_high2_CONV</code>
A_BXsmumu_lowq2	<code>SI_A_BXsmumu_lowq2</code> (double): Computes the low- q^2 forward-backward asymmetry of $B \rightarrow X_s \mu^+ \mu^-$.	<code>SuperIso_modelinfo</code>	<code>A_BXsmumu_lowq2_CONV</code>
A_BXsmumu_highq2	<code>SI_A_BXsmumu_highq2</code> (double): Computes the high- q^2 forward-backward asymmetry of $B \rightarrow X_s \mu^+ \mu^-$.	<code>SuperIso_modelinfo</code>	<code>A_BXsmumu_highq2_CONV</code>
A_BXsmumu_zero	<code>SI_A_BXsmumu_zero</code> (double): Computes the zero crossing q^2 value of the forward-backward asymmetry of $B \rightarrow X_s \mu^+ \mu^-$.	<code>SuperIso_modelinfo</code>	<code>A_BXsmumu_zero_CONV</code>
BRBXstautau_highq2	<code>SI_BRBXstautau_highq2</code> (double): Computes the inclusive high- q^2 branching fraction of $B \rightarrow X_s \tau^+ \tau^-$.	<code>SuperIso_modelinfo</code>	<code>BRBXstautau_highq2_CONV</code>
A_BXstautau_highq2	<code>SI_A_BXstautau_highq2</code> (double): Computes the high- q^2 forward-backward asymmetry of $B \rightarrow X_s \tau^+ \tau^-$.	<code>SuperIso_modelinfo</code>	<code>A_BXstautau_highq2_CONV</code>

Table 2: Observable capabilities of FlavBit that involve Wilson coefficients in their calculation (from `SuperIso` unless otherwise specified).

$$S_3 = \frac{1}{2} \frac{A_\perp^{L2} - A_\parallel^{L2}}{A_\parallel^2 + A_\perp^2 + A_0^2} + L \rightarrow R, \quad (12)$$

$$S_4 = \frac{1}{\sqrt{2}} \frac{\text{Re}(A_0^{L*} A_\parallel^L)}{A_\parallel^2 + A_\perp^2 + A_0^2} + L \rightarrow R, \quad (13)$$

$$S_5 = \sqrt{2} \frac{\text{Re}(A_0^{L*} A_\perp^L)}{A_\parallel^2 + A_\perp^2 + A_0^2} - L \rightarrow R, \quad (14)$$

$$A_{\text{FB}} = \frac{8}{3} \frac{\text{Re}(A_\perp^{L*} A_\parallel^L)}{A_\parallel^2 + A_\perp^2 + A_0^2} - L \rightarrow R, \quad (15)$$

$$S_7 = \sqrt{2} \frac{\text{Im}(A_0^{L*} A_\parallel^L)}{A_\parallel^2 + A_\perp^2 + A_0^2} + L \rightarrow R, \quad (16)$$

$$S_8 = \frac{1}{\sqrt{2}} \frac{\text{Im}(A_0^{L*} A_\perp^L)}{A_\parallel^2 + A_\perp^2 + A_0^2} + L \rightarrow R, \quad (17)$$

$$S_9 = \frac{\text{Im}(A_\perp^{L*} A_\parallel^L)}{A_\parallel^2 + A_\perp^2 + A_0^2} - L \rightarrow R. \quad (18)$$

The indices \perp , \parallel and 0 refer to the K^* (892) transversity amplitudes, while $L \rightarrow R$ refers to the chirality-flipped version of the previous term in each expression.

Capability	Function (Return Type): Brief Description	Dependencies	Backend requirements
<code>BKstarmumu_l_m</code>	<code>SI_BKstarmumu_l_m</code> (<code>Flav_KstarMuMu_obs</code>): Computes all observables associated with $B^0 \rightarrow K^{*0} \mu^+ \mu^-$ in a q^2 bin specified by l and m . See caption for details.	<code>SuperIso_modelinfo</code>	<code>SI_BKstarmumu_CONV</code>
<code>AI_BKstarmumu</code>	<code>SI_AI_BKstarmumu</code> (<code>double</code>): Computes the low- q^2 isospin asymmetry of $B \rightarrow K^* \mu^+ \mu^-$ (in GeV^2).	<code>SuperIso_modelinfo</code>	<code>AI_BKstarmumu_CONV</code>
<code>AI_BKstarmumu_zero</code>	<code>SI_AI_BKstarmumu_zero</code> (<code>double</code>): Computes the zero-crossing q^2 value of the isospin asymmetry of $B \rightarrow K^* \mu^+ \mu^-$.	<code>SuperIso_modelinfo</code>	<code>AI_BKstarmumu_zero_CONV</code>

Table 3: Observable capabilities of `FlavBit` related to the decay $B^0 \rightarrow K^{*0} \mu^+ \mu^-$. The indices l and m refer to the edges of the energy bin used in the particular function. The functions and capabilities are named such that $l, m = 11, 25$ indicates an energy range of $1.1\text{--}2.5 \text{ GeV}^2$, and so on. Possible pairs of l and m are (11,25), (25,40), (40,60), (60,80), (15,17) and (17,19); the last two refer to momentum transfer ranges of $15\text{--}17\text{--}19 \text{ GeV}^2$.

Name (type)	Description
<code>BR</code> (<code>double</code>)	branching fraction
<code>AFB</code> (<code>double</code>)	forward-backward asymmetry
<code>FL</code> (<code>double</code>)	longitudinal fraction
<code>S3</code> (<code>double</code>)	S_3
<code>S4</code> (<code>double</code>)	S_4
<code>S5</code> (<code>double</code>)	S_5
<code>S7</code> (<code>double</code>)	S_7
<code>S8</code> (<code>double</code>)	S_8
<code>S9</code> (<code>double</code>)	S_9
<code>q2_min</code> (<code>double</code>)	q^2 bin lower edge
<code>q2_max</code> (<code>double</code>)	q^2 bin upper edge

Table 4: Observables contained in the `Flav_KstarMuMu_obs` structure.

The amplitudes $A_{\perp, \parallel, 0}$ depend on form factors and Wilson coefficients, and can be written at leading order in QCD in the form:

$$A_{\perp}^{L,R} \propto \left\{ (C_9^{\text{eff}} + C_9^{\text{eff}'}) \mp (C_{10} + C'_{10}) \frac{V(q^2)}{m_B + m_{K^*}} + \frac{2m_b}{q^2} (C_7^{\text{eff}} + C_7^{\text{eff}'}) T_1(q^2) \right\}, \quad (19)$$

$$A_{\parallel}^{L,R} \propto \left\{ (C_9^{\text{eff}} - C_9^{\text{eff}'}) \mp (C_{10} - C'_{10}) \frac{A_1(q^2)}{m_B + m_{K^*}} + \frac{2m_b}{q^2} (C_7^{\text{eff}} - C_7^{\text{eff}'}) T_2(q^2) \right\}, \quad (20)$$

$$A_0^{L,R} \propto \left\{ [(C_9^{\text{eff}} - C_9^{\text{eff}'}) \mp (C_{10} - C'_{10})] \times [(m_B^2 - m_{K^*}^2 - q^2)(m_B + m_{K^*} A_1(q^2) - \lambda \frac{A_2(q^2)}{m_B + m_{K^*}})] + 2m_b(C_7^{\text{eff}} + C_7^{\text{eff}'}) \times [(m_B^2 + 3m_{K^*}^2 - q^2) T_2(q^2) - \frac{\lambda}{m_B^2 - m_{K^*}^2} T_3(q^2)] \right\}. \quad (21)$$

In the limit of large recoil (low q^2), the seven form factors $A_{1,2}$, $T_{1,2,3}$ and V can be replaced by only two form factors ξ_{\perp} and ξ_{\parallel} . This makes it possible to write a set of six observables that are independent of form factors in this approximation (see Ref. [50]). These are denominated⁶ $P_i^{(\prime)}$, with $i \in [1, 6]$. Some of these observables were independently proposed by other authors with a different name, e.g. $P_1 = A_T^{(2)}$ [51], $P_2 = 2 \times A_T^{Re}$ [52].

The observables P_i can be written as ratios of the observables F_L and S_i , therefore if the full form factors $A_{1,2}$, $T_{1,2,3}$, V [53] and their correlations are used it is equivalent to using the full set of P_i observables. One of the most interesting measurements in these decays is the observable P'_5 , which shows a deviation with respect to the SM prediction of about 4σ in the region $4 < q^2/\text{GeV}^2 < 8$ [18, 23, 47]. The most accredited explanation for this deviation is a reduced $C_9^{\text{eff}}(q^2)$ Wilson coefficient, but it is not yet clear if this is due to hadronic uncertainties [54–57] or a genuine contribution from new physics [58–61]. In `FlavBit`, we incorporate a 10% theoretical uncertainty (at the amplitude level) into our correlation matrix for $B^0 \rightarrow K^{*0} \mu^+ \mu^-$ observables, to account for errors arising from non-factorisable power corrections [62].

As set out in Tables 3 and 4, `FlavBit` can calculate the full suite of observables for $B^0 \rightarrow K^{*0} \mu^+ \mu^-$, in six different q^2 bins over the range $1.1 \leq q^2/\text{GeV}^2 \leq 19.0$. These are provided by the capabilities `BKstarmumu_l_m`, where the lower q^2 bin edge is denoted by l and the upper edge by m . The functions with these capabilities return a `Flav_KstarMuMu_obs` object (Table 4), which contains the overall branching fraction, forward-backward asymmetry and detailed angular observables F_L , S_3 , S_4 , S_5 , S_7 , S_8 and S_9 . These observables can either be extracted manually from the `Flav_KstarMuMu_obs` object itself, or output

⁶Note that for historical reasons the observables $P'_{4,5,6}$ carry a $'$.

in full via the GAMBIT printer system [4] for later analysis.

The angular analysis of $B^0 \rightarrow K^{*0}\ell^+\ell^-$ [63] at much lower momentum transfer ($q^2 \lesssim 1 \text{ GeV}^2$) can also provide strong constraints, specifically on the coefficients $C_7^{(\prime)}$. However, experimental analyses of $B^0 \rightarrow K^{*0}\mu^+\mu^-$ in this regime are impacted by the assumption that the muon is massless. We therefore do not include this lower angular bin in FlavBit.

Asymmetries between B^0 and \bar{B}^0 in $B^0 \rightarrow K^{*0}\mu^+\mu^-$ have also been measured by the LHCb collaboration [47]. These are important for constraining the imaginary parts of a number of Wilson Coefficients.

Another observable useful for isolating the contribution of new physics, owing to its insensitivity to hadronic parameters such as form factors, is the CP -averaged $B \rightarrow K^*\mu^+\mu^-$ isospin asymmetry [64],

$$\frac{dA_I}{dq^2} \equiv \frac{d\Gamma_{B^0 \rightarrow K^{*0}\mu^+\mu^-}/dq^2 - d\Gamma_{B^\pm \rightarrow K^{*\pm}\mu^+\mu^-}/dq^2}{d\Gamma_{B^0 \rightarrow K^{*0}\mu^+\mu^-}/dq^2 + d\Gamma_{B^\pm \rightarrow K^{*\pm}\mu^+\mu^-}/dq^2}. \quad (22)$$

FlavBit provides the integrated low- q^2 asymmetry, corresponding to the integral of Eq. 22 over the range $1 \leq q^2/\text{GeV}^2 \leq 6$ (`AI_BKstarmumu` in Table 3). It also computes the zero-crossing of the asymmetry, corresponding to the q^2 value where the differential decay rates of $B^0 \rightarrow K^{*0}\mu^+\mu^-$ and $B^\pm \rightarrow K^{*\pm}\mu^+\mu^-$ are equal (`AI_BKstarmumu_zero` in Table 3).

The measurement of the inclusive branching fraction of $B \rightarrow X_s\ell^+\ell^-$ is challenging from the experimental point of view, however has several theory advantages. The differential decay rate at leading order in QCD can be written as (see Ref. [65] and references therein):

$$\begin{aligned} \frac{d\mathcal{B}(B \rightarrow X_s\ell^+\ell^-)}{d\hat{s}} &= \mathcal{B}(B \rightarrow X_c\ell\bar{\nu}) \frac{\alpha^2}{4\pi^2 f(z)} \frac{|V_{tb}V_{ts}^*|^2}{|V_{cb}|^2} \\ &\times (1-\hat{s})^2 \sqrt{1 - \frac{4m_\ell^2}{q^2}} \left\{ (|C_9^{\text{eff}}|^2 + |C_{10}|^2) (1+2\hat{s}) \right. \\ &\quad \left. + 4|C_7^{\text{eff}}|^2 \left(1 + \frac{2}{\hat{s}}\right) + 12 \text{Re}(C_7^{\text{eff}}C_9^{\text{eff}}) \right\} \quad (23) \end{aligned}$$

where $\hat{s} \equiv q^2/m_b^2$, $z = m_c^2/m_b^2$ and

$$f(z) = 1 - 8z + 8z^3 - z^4 - 12z^2 \ln z. \quad (24)$$

The inclusive and differential branching fractions of $B \rightarrow X_s\ell^+\ell^-$ were measured at B factories [66–69].

As detailed in Table 2, FlavBit computes predictions for $\mathcal{B}(B \rightarrow X_s\mu^+\mu^-)$, integrated over both high and low q^2 ranges (capabilities `BRBXsmumu_highq2` and

`BRBXsmumu_lowq2`). It also computes the branching fraction at high q^2 for the equivalent process with τ leptons in the final state, $\mathcal{B}(B \rightarrow X_s\tau^+\tau^-)$ (capability `BRBXstautau_highq2`).

A complementary $B \rightarrow X_s\ell^+\ell^-$ angular observable is the forward-backward asymmetry $A_{\text{FB},B \rightarrow X_s\ell^+\ell^-}$, defined differentially with respect to \hat{s} as

$$A_{\text{FB},B \rightarrow X_s\ell^+\ell^-}(\hat{s}) \equiv \int_0^1 \frac{d\mathcal{B}(\hat{s}, z)}{d\hat{s}dz} - \int_{-1}^0 \frac{d\mathcal{B}(\hat{s}, z)}{d\hat{s}dz}, \quad (25)$$

where z is the cosine of the forward angle. FlavBit computes the $B \rightarrow X_s\mu^+\mu^-$ integrated forward-backward asymmetry at both low and high q^2 (capabilities `A_BXsmumu_highq2` and `A_BXsmumu_lowq2`), along with the zero-crossing of the asymmetry, corresponding the q^2 value for which the asymmetry vanishes (`A_BXsmumu_zero`). It also predicts the asymmetry of the equivalent process involving τ leptons at high q^2 (capability `A_BXstautau_highq2`).

The decay $B_s \rightarrow \phi\mu^+\mu^-$ is described by the same formalism as $B \rightarrow K^*\mu^+\mu^-$. However, while the latter is a self-tagging decay, i.e. the flavour of the B meson at decay time can be inferred by the charge of the kaon coming from the decay of the $K^*(892)$, this is not the case for the $B_s \rightarrow \phi\mu^+\mu^-$. This implies that when averaging between B_s and \bar{B}_s , some terms of the angular distributions (including P'_5) vanish. The branching ratios of both $B_s \rightarrow \phi\mu^+\mu^-$ and the related decay $B^+ \rightarrow K^+\mu^+\mu^-$ are sensitive to BSM physics, mainly via the Wilson coefficients $C_9^{(\prime)}$ and $C_{10}^{(\prime)}$. The measurement of the branching fraction of $B_s \rightarrow \phi\mu^+\mu^-$ by the LHCb experiment [15] is also in tension with respect to SM predictions. We do not include these channels directly in FlavBit, because to do so rigorously would require the ability to recompute model-dependent BSM contributions to theoretical uncertainties. This is a capability that we anticipate including in a future version of FlavBit.

In addition, angular measurements of the decay $B^0 \rightarrow K\pi\mu^+\mu^-$ outside the $K^*(892)$ resonance have been recently performed [70], however we do not yet have enough knowledge of the different K^* resonances in that region of $K\pi$ invariant mass to interpret the result in terms of Wilson coefficients [71]. For this reason, the decays $B^0 \rightarrow K\pi\mu^+\mu^-$ outside the $K^*(892)$ are not yet implemented in FlavBit.

Lepton flavour universality in $b \rightarrow s$ transitions has also been tested by measuring the ratio $R_K = \frac{\mathcal{B}(B^+ \rightarrow K^+\mu^+\mu^-)}{\mathcal{B}(B^+ \rightarrow K^+e^+e^-)}$. A tension corresponding to 2.6σ was observed [17]. Contrary to the anomalies in the aforementioned $b \rightarrow s\ell\ell$ transitions, the tension in R_K cannot be explained by hadronic uncertainties. Accommodating lepton flavour non-universality within the effective

Hamiltonian framework of Eq. 2 requires splitting operators $\mathcal{O}_9^{(\prime)}$ and $\mathcal{O}_{10}^{(\prime)}$ into separate effective operators for different leptons. In the context of this expanded treatment, the so-called flavour anomalies in rare decays seem to form a coherent pattern, with a reduction of about 25% observed in the muonic C_9 Wilson coefficient relative to the SM prediction. In general these scenarios are not easy to accommodate within the MSSM, although a global agreement at the 2σ level is still possible [72]. Presently, FlavBit does not deal with violations of lepton flavour universality, so R_K is not yet included as an observable.

4.4 Rare purely leptonic decays

Like its penguin counterparts $B \rightarrow X\ell^+\ell^-$, the rare leptonic decay $B_s^0 \rightarrow \ell^+\ell^-$ also probes the FCNC $b \rightarrow s$ transition, and is proportional to the CKM entries V_{tb} and V_{ts} . Similarly, $B^0 \rightarrow \ell^+\ell^-$ probes $b \rightarrow d$ and is proportional to V_{tb} and V_{td} . These are rather clean channels from the theoretical perspective, as the main uncertainty comes only from the meson decay constant, which can be calculated in lattice QCD. The branching fraction of these decays is

$$\begin{aligned} \mathcal{B}(B_q^0 \rightarrow \ell^+\ell^-) &= \frac{G_F^2 \alpha^2}{64\pi^3} f_{B_q}^2 \tau_{B_q} m_{B_q}^3 |V_{tb} V_{tq}^*|^2 \\ &\times \sqrt{1 - \frac{4m_\ell^2}{m_{B_q}^2}} \left\{ \left(1 - \frac{4m_\ell^2}{m_{B_q}^2}\right) |C_{Q1} - C'_{Q1}|^2 \right. \\ &\left. + \left| (C_{Q2} - C'_{Q2}) + 2 \frac{m_\ell}{m_{B_q}} (C_{10} - C'_{10}) \right|^2 \right\}. \end{aligned} \quad (26)$$

Because the B meson is a pseudoscalar, these decays are helicity-suppressed, in addition to the GIM suppression. Therefore, in the SM and in all lepton-flavour-universal $V \pm A$ models, the ratio of the branching fractions for different leptons is given by:

$$\frac{\mathcal{B}(B_q \rightarrow \ell_1^+ \ell_1^-)}{\mathcal{B}(B_q \rightarrow \ell_2^+ \ell_2^-)} = \frac{m_1^2}{m_2^2}, \quad (27)$$

where $m_{1(2)}$ is the mass of the lepton $\ell_{1(2)}$. These decays set strong constraints on models with extended Higgs sectors such as the 2HDM, as scalar contributions would alleviate the helicity suppression. Such decays are also sensitive to new bosons with $V \pm A$ couplings (e.g. W' and W_R), which would modify the Wilson coefficients $C_{10}^{(\prime)}$ of the SM.

FlavBit has the capability to compute the branching fraction for $B^0 \rightarrow \mu^+\mu^-$ (`Bmumu` in Table 2), as well as for (CP -averaged) B_s decays to e^+e^- and $\mu^+\mu^-$ (`Bsee_untag` and `Bsmumu_untag`). The latter can also be obtained in the MSSM and SM from FeynHiggs via the `FH_FlavourObs` capability (see Tables 1 and 5).

Name	Description
<code>Bsg_MSSM (fh_real)</code>	Total inclusive branching fraction of $B \rightarrow X_s \gamma$ in the MSSM
<code>Bsg_SM (fh_real)</code>	Total inclusive branching fraction of $B \rightarrow X_s \gamma$ in the SM
<code>DeltaMs_MSSM (fh_real)</code>	$B_s^0 - \bar{B}_s^0$ mass difference in the MSSM
<code>DeltaMs_SM (fh_real)</code>	$B_s^0 - \bar{B}_s^0$ mass difference in the SM
<code>Bsmumu_MSSM (fh_real)</code>	Branching fraction of $B_s^0 \rightarrow \mu^+\mu^-$ in the MSSM
<code>Bsmumu_SM (fh_real)</code>	Branching fraction of $B_s^0 \rightarrow \mu^+\mu^-$ in the SM

Table 5: Flavour observables contained in the `fh_FlavourObs` structure obtained from FeynHiggs.⁷

4.5 Other flavour observables

Other observables included in FlavBit are $B \rightarrow X_s \gamma$, the ratio $R_\mu = \frac{\mathcal{B}(K \rightarrow \mu\nu\mu)}{\mathcal{B}(\pi \rightarrow \mu\nu\mu)}$, and the meson mixing ΔM_s .

Radiative decays of B mesons are important to constrain the electromagnetic operator and the corresponding Wilson coefficients $C_7^{(\prime)}$. The main constraint comes from the measurement of the inclusive decay $B \rightarrow X_s \gamma$ [73, 74]. The prediction of this branching fraction is relatively clean, and benefits from the Heavy Quark Expansion in the same way as the $B \rightarrow X_s \ell^+\ell^-$ process.

The branching ratio can be written at leading order as

$$\mathcal{B}(\bar{B} \rightarrow X_s \gamma) = \mathcal{B}(\bar{B} \rightarrow X_c e \bar{\nu})_{\text{exp}} \left| \frac{V_{ts}^* V_{tb}}{V_{cb}} \right|^2 \frac{6\alpha}{\pi C} |C_7^{\text{eff}}|^2, \quad (28)$$

where $\mathcal{B}(\bar{B} \rightarrow X_c e \bar{\nu})_{\text{exp}}$ is the experimentally-measured value of the branching fraction for $\bar{B} \rightarrow X_c e \bar{\nu}$, and

$$C = \left| \frac{V_{ub}}{V_{cb}} \right|^2 \frac{\mathcal{B}(\bar{B} \rightarrow X_c e \bar{\nu})}{\mathcal{B}(\bar{B} \rightarrow X_u e \bar{\nu})}. \quad (29)$$

This measurement sets constraints on the charged Higgs mass and couplings of the 2HDM [75–78]. In addition, these measurements constrain models with additional neutral gauge bosons such as the Z' [35]. FlavBit implements this observable as `bsgamma` (Table 2), and within the `FH_FlavourObs` capability (see Tables 1 and 5).

The exclusive decays $B \rightarrow K^* \gamma$ and $B_s \rightarrow \phi \gamma$ also constrain the coefficients $C_7^{(\prime)}$, but their impact is not

⁷Note that the branching fraction of $B \rightarrow X_s \gamma$ is ill-defined for $E_\gamma \rightarrow 0$, due to the IR divergence associated with soft photon emission. Although the adopted cutoff on E_γ is unspecified in FeynHiggs, $\mathcal{B}(B \rightarrow X_s \gamma)$ here appears to follow the definition of ‘total’ advocated in Ref. [79], with $E_\gamma > m_b/10 \sim 0.4$ GeV.

yet competitive with the inclusive one. However, the inclusive decays can only constrain the sum of $|C_7|^2$ and $|C_7'|^2$. The best constraint on the right-handed current C_7' contribution presently comes from the angular analysis of $B^0 \rightarrow K^{*0} \ell^+ \ell^-$ at low q^2 (see Sec. 4.3). In FlavBit, we provide the CP -averaged isospin asymmetry of $B \rightarrow K^* \gamma$ decays [80],

$$\Delta_0 \equiv \frac{\Gamma(\bar{B}^0 \rightarrow \bar{K}^{*0} \gamma) - \Gamma(B^\pm \rightarrow K^{*\pm} \gamma)}{\Gamma(\bar{B}^0 \rightarrow \bar{K}^{*0} \gamma) + \Gamma(B^\pm \rightarrow K^{*\pm} \gamma)}, \quad (30)$$

as a calculable observable, as it can receive contributions from charged Higgs bosons and any other new fields with similar quantum numbers (such as charginos in supersymmetry) [81]. The predicted asymmetry can be accessed via capability `delta0` (Table 2).

The leptonic decays of K and π mesons are also sensitive to the existence of charged Higgs bosons [82]. FlavBit computes the ratio [83]

$$\begin{aligned} R_\mu &= \frac{\mathcal{B}(K \rightarrow \mu \nu_\mu)}{\mathcal{B}(\pi \rightarrow \mu \nu_\mu)} \\ &= (1 + \delta_{\text{em}}) \frac{\tau_K}{\tau_\pi} \left| \frac{V_{us}}{V_{ud}} \right|^2 \frac{f_K^2}{f_\pi^2} \frac{m_K}{m_\pi} \left(\frac{1 - m_\ell^2/m_K^2}{1 - m_\ell^2/m_\pi^2} \right)^2 \\ &\quad \times \left[1 - \frac{m_{K^+}^2}{M_{H^+}^2} \left(1 - \frac{m_d}{m_s} \right) \frac{\tan^2 \beta}{1 + \epsilon_0 \tan \beta} \right]^2, \quad (31) \end{aligned}$$

which has a smaller theoretical uncertainty than the individual decays. Here $\delta_{\text{em}} = 0.0070 \pm 0.0035$ is a long-distance electromagnetic correction factor. We also consider the quantity $R_{\mu 23}$ [83],

$$\begin{aligned} R_{\mu 23} &= \left| \frac{V_{us}(K\ell 2)}{V_{us}(K\ell 3)} \times \frac{V_{ud}(0^+ \rightarrow 0^+)}{V_{ud}(\pi\ell 2)} \right| \\ &= \left| 1 - \frac{m_{K^+}^2}{M_{H^+}^2} \left(1 - \frac{m_d}{m_s} \right) \frac{\tan^2 \beta}{1 + \epsilon_0 \tan \beta} \right|, \quad (32) \end{aligned}$$

where ℓ_i refers to leptonic decays with i particles in the final state, and $0^+ \rightarrow 0^+$ corresponds to nuclear beta decay. These are provided by capabilities `Rmu` and `Rmu23`, respectively, and the relevant functions are detailed in Table 1.

It is well known that neutral meson systems are characterised by a rich phenomenology. In general, eigenstates of flavour are not eigenstates of mass, causing neutral mesons to oscillate. The parameters governing oscillations are the difference in mass between the heavy and light eigenstates $\Delta M = M_H - M_L$ and the difference in their decay widths $\Delta\Gamma = \Gamma_H - \Gamma_L$. While in the neutral kaon system the difference in lifetime is very large, so we denote the two states ‘short’ (K_S^0) and ‘long’ (K_L^0), in the neutral B system $\Delta\Gamma \ll \Delta M$, so it is more suitable to call them ‘heavy’ and ‘light’. The oscillation frequency is related to the difference in mass

ΔM_q , which for the neutral B meson is

$$\Delta M_q = \frac{G_F^2}{6\pi^2} \eta_B m_{B_q} (\hat{B}_q f_{B_q}^2) M_W^2 S_0(x_t) |V_{tq}|^2, \quad (33)$$

where \hat{B}_q is the renormalisation-group-invariant parameter, f_{B_q} is the B_q decay constant and $S_0(x_t)$ is a simple function of the top mass. The hadronic parameter f_{B_q} is the same factor that appears in the branching fraction of $B_q \rightarrow \ell^+ \ell^-$ decays (Eq. 26). The branching fractions and mass differences are therefore related as [84]

$$\frac{\mathcal{B}(B_s^0 \rightarrow \ell^+ \ell^-)}{\mathcal{B}(B^0 \rightarrow \ell^+ \ell^-)} = \frac{\hat{B}_s \tau(B_s^0) \Delta M_s}{\hat{B}_d \tau(B^0) \Delta M_d}. \quad (34)$$

In FlavBit, ΔM_s can be obtained in either the SM or MSSM, via the `FH_FlavourObs` capability (see Tables 1 and 5).

5 Likelihoods

After calculating the observables described in Section 4, FlavBit can be used to compute likelihoods based on a comparison of the predictions with current experimental measurements.

The experimental results and theoretical errors are stored in a YAML database. Taking the branching fraction of $B_s \rightarrow \mu^+ \mu^-$ as an example, the FlavBit database entry is

```
- name: BR_Bs2mumu
  islimit: false
  exp_value: 3.0e-9
  exp_stat_error: 0.6e-9
  exp_sys_error: 0.25e-9
  exp_source: 1703.05747
  th_error: 0.1
  th_error_type: M
  th_error_source: 1208.0934
  correlation:
  - name: NONE
```

The individual fields available in such entries are described in detail in Table 6. Note in particular that the theory error may be given either as a fraction, as in this example, or as an absolute value. The `Flav_reader` object is responsible for reading the experimental results and theoretical errors, and calculating the resulting covariance matrix. Table 7 describes its specific functions.

We consider correlated theoretical and experimental uncertainties separately, building two covariance matrices and assuming linear correlations for both. In the case of asymmetric uncertainties, we symmetrise the errors by taking the mean of the upper and lower uncertainties. FlavBit constructs the experimental covariance matrix directly from the `exp_stat_error`, `exp_sys_error` and `correlation` entries in its YAML database (Table 6

Name	Description
<code>name</code>	Unique name of a given measurement
<code>islimit</code>	Flag that indicates if the measurement is in the form of an upper limit (<code>true</code>) or a measurement (<code>false</code>)
<code>exp_value</code>	The experimental measurement (if <code>islimit = false</code>) or limit (if <code>islimit = true</code>)
<code>exp_stat_error</code>	1σ uncorrelated statistical uncertainty on the experimental measurement or limit
<code>exp_sys_error</code>	1σ uncorrelated systematic uncertainty on the experimental measurement or limit
<code>exp_source</code>	The source of the experimental value and uncertainties
<code>th_error</code>	1σ uncorrelated theoretical uncertainty
<code>th_error_type</code>	Flag indicating whether the theory error is multiplicative (<code>M</code>) or additive (<code>A</code>).
<code>th_source</code>	The source of the theoretical uncertainty
<code>correlation</code>	Sub-section with correlations of the experimental measurement/limit to other experimental measurements/limits: <ul style="list-style-type: none"> <code>name</code> Name of another measurement with which this one is correlated <code>value</code> Correlation matrix entry relating the two measurements <code>name</code> Name of a third measurement with which this one is correlated <code>value</code> etc

Table 6: Parameters of a single experimental entry in the FlavBit YAML database.

Name	Description
<code>int read_yaml(str name)</code>	Reads an entire YAML database file <code>name</code> into memory.
<code>void read_yaml_measurement(str name, str measurement_name)</code>	Extracts a single measurement <code>measurement_name</code> from the YAML database file <code>name</code> .
<code>void debug_mode(bool debug)</code>	Turns on (<code>debug = true</code>) or off (<code>debug = false</code>) printing of all parameters.
<code>void create_global_corr()</code>	Constructs a total correlation matrix from all measurements read in.
<code>void print_corr_matrix()</code>	Prints the constructed correlation matrix.
<code>void print_cov_matrix()</code>	Prints the corresponding covariance matrix.
<code>void print_cov_inv_matrix()</code>	Prints the inverse of the covariance matrix.
<code>matrix(n,n) get_cov()</code>	Returns the experimental covariance matrix covering all measurements read in.
<code>matrix(n,1) get_exp_value()</code>	Returns the central experimental values for all measurements read in.
<code>matrix(n,1) get_th_err()</code>	Returns the central (uncorrelated) theory error for each of the measurements read in.

Table 7: Important methods of the FlavBit `Flav_reader` class. Here `str` is an alias for `std::string`, `n` is the number of measurements so far read in by the `Flav_reader` instance, and `matrix(x,y)` is an $x \times y$ `boost::numeric::ublas::matrix<double>`.

and example above). It takes the `th_error` entries in the YAML database and uses them to populate the diagonal of the theory covariance matrix. It determines the off-diagonal terms on a case-by-case basis in each likelihood function, in order to make it possible for different likelihood functions to adjust the correlations according to whether different nuisance parameters are scanned over directly, or should be included via the correlation matrix.⁸

⁸Users of FlavBit should be aware of a potential pitfall arising from this arrangement. The theory uncertainties and correlations that we include in the current release and describe in this paper already incorporate uncertainties on input parameters such as form factors, decay constants, SM masses and couplings, and in particular, CKM matrix entries. The SM masses and couplings are sufficiently well constrained that any error term dominated by them can be safely neglected, and generally is in FlavBit, seeing as they can be easily varied within GAMBIT as nuisance parameters. On the other hand, CKM elements

FlavBit builds the full covariance matrix by summing the experimental and theoretical covariance matrices. If an observable and its measurements are uncorrelated with other observables, the resulting uncertainty then becomes simply the sum in quadrature of the theoretical and experimental errors.

We determine likelihoods for flavour observables under the assumption of correlated Gaussian errors and Wilks' Theorem, taking (twice) the final log-likelihood

are substantial and dominant contributors to the error budget of some processes. The current likelihoods in FlavBit should therefore *not* be employed in any scan where CKM elements are varied as nuisance parameters, without first carefully considering which likelihood terms already include their impact, and either removing those observables from the fit, or reducing the theory errors accordingly.

Capability	Function (Return Type): Brief Description	Dependencies
SL_M	<code>SL_measurements</code> (<code>predictions_measurements_covariances</code>): Tree-level leptonic and semi-leptonic decay predictions, measurements and covariances.	RD RDstar BDmunu BDstarmunu Btaunu Dstauunu Dsmunu Dmunu
SL_LL	<code>SL_likelihood</code> (<code>double</code>): Log-likelihood for tree-level leptonic and semi-leptonic decays.	SL_M
b2s1l_M	<code>b2s1l_measurements</code> (<code>predictions_measurements_covariances</code>): Electroweak penguin decay predictions, measurements and covariances.	BKstarmumu_11_25 BKstarmumu_25_40 BKstarmumu_40_60 BKstarmumu_60_80 BKstarmumu_15_17 BKstarmumu_17_19
b2s1l_LL	<code>b2s1l_likelihood</code> (<code>double</code>): Log-likelihood for electroweak penguin decays, including angular observables.	b2s1l_M
b21l_M	<code>b21l_measurements</code> (<code>predictions_measurements_covariances</code>): Rare purely leptonic decay predictions, measurements and covariances.	Bsmumu_untag Bmumu
b21l_LL	<code>b21l_likelihood</code> (<code>double</code>): Log-likelihood for rare purely leptonic decays.	b21l_M
b2sgamma_LL	<code>b2sgamma_likelihood</code> (<code>double</code>): Log-likelihood for the branching fraction of $B \rightarrow X_s \gamma$.	bsgamma
deltaMB_LL	<code>deltaMB_likelihood</code> (<code>double</code>): Log-likelihood for B meson mass asymmetries.	deltaMs

Table 8: Likelihood capabilities of FlavBit. All measurement functions (capabilities ending in `_M`) return experimental and theoretical central values, as well as experimental and theoretical covariance matrices.

to be χ^2 distributed. This gives

$$\log \mathcal{L} = -\frac{1}{2}\chi^2 = -\frac{1}{2} \sum_{i,j=1}^N (y_i - x_i) V_{ij}^{-1} (y_j - x_j), \quad (35)$$

where x_i is the experimental measurement of the i th observable, y_i is the i th theory prediction and V^{-1} is the inverse of the full covariance matrix.

FlavBit contains five different likelihood functions. These correspond to different likelihood classes within which observables might be correlated.

`SL_likelihood`: tree level leptonic and semi-leptonic B and D decays ($B^\pm \rightarrow \tau \nu$, $D_{(s)}^\pm \rightarrow \ell \nu_\ell$, $B \rightarrow D^{(*)} \ell \nu_\ell$)

`b2s1l_likelihood`: electroweak penguin decays ($B \rightarrow X_s \ell^+ \ell^-$)

`b21l_likelihood`: rare purely leptonic B decays ($B_{(s)}^0 \rightarrow \ell^+ \ell^-$)

`b2sgamma_likelihood`: rare radiative B decays ($B \rightarrow X_s \gamma$)

`deltaMB_likelihood`: B meson mass asymmetries

The likelihood functions, their capabilities and dependencies are given in Table 8. In the following subsections, we give details of the experimental data included in each.

5.1 Tree-level leptonic and semi-leptonic likelihood

We take the branching fractions of the decays $B \rightarrow D^{(*)} \ell \nu_\ell$ from the PDG [28], which combines results from many experiments but is dominated by the contributions from BaBar [85, 86] and Belle [87, 88].

BaBar [19, 20] and Belle [21, 89, 90] also recently measured the ratios $R_{D^{(*)}} \equiv \mathcal{B}(B \rightarrow D^{(*)} \tau \nu_\tau) / \mathcal{B}(B \rightarrow D^{(*)} \ell \nu_\ell)$. LHCb also measured R_{D^*} for the muonic final state [16]. The average of these measurements, assuming lepton flavour universality between muons and electrons, has been computed by the HFAG collaboration [91, 92] and is included in FlavBit:

$$R_D = 0.403 \pm 0.040 \pm 0.024, \quad (36)$$

$$R_{D^*} = 0.310 \pm 0.015 \pm 0.008. \quad (37)$$

Compared to the SM predictions of $R_D = 0.300 \pm 0.008$ [93] and $R_{D^*} = 0.252 \pm 0.003$ [94], a total discrepancy of about 4σ is observed. We take the experimental correlation between R_D and R_{D^*} , arising from common systematics in the measurements, from Ref. [91]. The theory uncertainties are considered uncorrelated; we take these from Refs. [95, 96].

In addition to R_D and R_{D^*} , we also explicitly include in the likelihood the decays $B \rightarrow D^{(*)} \mu \nu$, adopting the

experimental values from the PDG [28]. Taken with R_D and R_{D^*} , this set of four likelihood terms constitutes a complete basis for the models of lepton non-universality. The theory errors for the $B \rightarrow D^{(*)}\mu\nu$ branching fractions are dominated by form factors [29, 93]. Performing a detailed error analysis with `SuperIso` gives a theoretical uncertainty of 9% for $B \rightarrow D\mu\nu$ and 11% for $B \rightarrow D^*\mu\nu$.

Experiments have not measured any correlation between the muonic and tauonic modes of the decays contributing to $R_{D^{(*)}}$. However, the theory systematics are strongly correlated; in our analysis with `SuperIso`, we find anti-correlations at the level of 55% for $B \rightarrow D\mu\nu$ and R_D , and 62% for $B \rightarrow D^{(*)}\mu\nu$ and R_{D^*} . These data are all included in the `FlavBit` likelihood.

For $B^\pm \rightarrow \ell\nu_\ell$, `FlavBit` uses experimental measurements from the PDG [28],

$$\mathcal{B}(B^+ \rightarrow \tau^+\nu_\mu) = (1.09 \pm 0.24) \times 10^{-4}. \quad (38)$$

This average is dominated by results from the BaBar [97, 98] and Belle [99, 100] experiments, and is in agreement with the SM. We take this measurement to be uncorrelated with all other measurements. The dominant theoretical uncertainty comes from the CKM element V_{ub} . The present uncertainty on this element is 9.5% [28], giving an overall theoretical uncertainty of 19%.

For the branching fractions of the $D_{(s)}^\pm$ decays $D^\pm \rightarrow \mu\nu_\mu$, $D_s^\pm \rightarrow \tau\nu_\tau$ and $D_s^\pm \rightarrow \mu\nu_\mu$, we adopt the experimental values of the PDG [28]. (`FlavBit` does not include $D^\pm \rightarrow \tau\nu_\tau$ as an observable, as its decay branching fraction has not yet been measured.) The theory errors on the $D_{(s)}^\pm$ decays are dominated by the knowledge of the decay constant of the corresponding charmed mesons, f_D and f_{D_s} . This leads to a theoretical uncertainty on the branching fractions of 3% for D^\pm decays and 2% for D_s^\pm decays [28].

As shown in Table 8, `FlavBit` collects together into `SL_M` the measured values, experimental correlations, theoretical predictions and theory uncertainties for $B^\pm \rightarrow \ell\nu_\ell$, the four $B \rightarrow D^{(*)}\ell\nu_\ell$ observables, and the three $D_{(s)}^\pm$ decays. This fills the only dependency of the final tree-level leptonic and semi-leptonic likelihood, which can be accessed via capability `SL_LL`.

5.2 Electroweak penguin likelihood

The electroweak penguin likelihood in `FlavBit` is calculated using the angular observables of the $B^0 \rightarrow K^{*0}\mu^+\mu^-$ decay, as measured by LHCb [47] in dimuon invariant mass squared bins of (1.1, 2.5), (2.5, 4), (4, 6), (6, 8), (15, 17) and (17, 19) GeV². The bin (11, 12.5) GeV² cannot be used in the likelihood, as the relative phase between the charmonium resonances in this

bin and the non-resonant decay is not currently known. We do not implement the measurements of Belle [23], as their contribution to the likelihood is negligible compared to the LHCb measurement. ATLAS and CMS have also very recently presented preliminary Run I measurements of the $B^0 \rightarrow K^{*0}\mu^+\mu^-$ angular observables [101, 102]; these data will be included in a future release of `FlavBit`.

For each q^2 bin, the `FlavBit` likelihood includes components arising from `FL`, `S3`, `S4`, `S5`, `AFB`, `S7`, `S8` and `S9`. It accounts for experimental correlations between these measurements within each bin, but assumes that measurements are not correlated across q^2 bins, as the uncertainty is dominated by the statistical component. The full correlation matrices within each bin are available publicly from LHCb [47] and included in the `FlavBit` YAML database. We include theory-induced correlated uncertainties between different angular observables for the same q^2 range from Ref. [62, 103].

The branching fractions for $B^0 \rightarrow K^{*0}\mu^+\mu^-$ decays are not part of the electroweak penguin likelihood in `FlavBit` 1.0.0, but are slated for inclusion in a future version, following the next update from LHCb. The isospin asymmetry of the $B^0 \rightarrow K^{*0}\mu^+\mu^-$ decay is non-trivially correlated with the angular observables, so we also do not include the corresponding observables (`AI_BKstarmumu` and `AI_BKstarmumu_zero` in Table 3) in the likelihood function.

Predictions of the branching fractions and forward-backward asymmetries of the inclusive decays $B \rightarrow X_s\mu^+\mu^-$ and $B \rightarrow X_s\tau^+\tau^-$, corresponding to the last 7 observables of Table 2, have lower theoretical uncertainties than those of $B^0 \rightarrow K^{*0}\mu^+\mu^-$. They are however not included in the `FlavBit` electroweak penguin likelihood, as they provide little additional constraining power when $B \rightarrow X_s\gamma$ is already included in a fit — and only $B \rightarrow X_s\ell^+\ell^-$ (where ℓ does not distinguish between e and μ) and its forward-backward asymmetry have been measured by BaBar and Belle [66–69], with higher uncertainties than measurements of the exclusive modes. We expect to include likelihoods for these observables in a future revision of `FlavBit`.

`FlavBit` reads the experimental measurements and correlations, collects them together with the theoretical predictions and uncertainties, and publishes them to the rest of `GAMBIT` under the capability `b2s11_M`. `FlavBit` then uses the measurements and correlations to compute the electroweak penguin decay likelihood, which is assigned capability `b2s11_LL`. See Table 8 for more details.

5.3 Rare purely leptonic likelihood

Experimentally, only the decays with muons in the final state have been observed, and therefore give the strongest constraints. For $B_s^0 \rightarrow \mu^+\mu^-$, we adopt the latest result from LHCb [104],

$$\mathcal{B}(B_s^0 \rightarrow \mu^+\mu^-) = (3.0 \pm 0.6_{-0.2}^{+0.3}) \times 10^{-9}. \quad (39)$$

For $B^0 \rightarrow \mu^+\mu^-$, we take the results of Ref. [105], which combines the measurements of the LHCb [106] and CMS experiments [107],

$$\mathcal{B}(B^0 \rightarrow \mu^+\mu^-) = (3.9_{-1.4}^{+1.6}) \times 10^{-10}. \quad (40)$$

Experimental correlations between the two decays are negligible [104].

Although the ATLAS collaboration have also recently measured these two branching fractions [108], they do not yet report a 3σ evidence for these decays. We thus do not include the ATLAS result in `FlavBit` at this stage. The similar decays $B_{(s)}^0 \rightarrow e^+e^-$ and $B_{(s)}^0 \rightarrow \tau^+\tau^-$ have not been measured to date. Only weak upper limits exist in these cases [109–111], which are currently much less constraining for models of new physics than the muon channels; we therefore do not include them in the `FlavBit` likelihood.

From the theoretical point of view, $B_{(s)}^0 \rightarrow \mu^+\mu^-$ decays are rather clean. The theory uncertainty is 10%, and is dominated by the knowledge of the meson decay constant f_{B_s} [112]. This is far smaller than the experimental uncertainty, and therefore has little impact. We also neglect corresponding correlations in the theoretical uncertainties associated with the two decays.

`FlavBit` reads the experimental measurements and theory errors, collects them together with the theoretical predictions, and publishes them to the rest of `GAMBIT` as `b211_M`. It then computes the rare purely leptonic decay likelihood from the measurements and uncertainties, and labels it with capability `b211_LL`. Table 8 gives full details.

5.4 Rare radiative B decay likelihood

`FlavBit` includes the average [78] of the measurements of $B \rightarrow X_s\gamma$ from BaBar [113–115] and Belle [116, 117] for $E_\gamma > 1.6$ GeV,

$$\mathcal{B}(B \rightarrow X_s\gamma) = (3.27 \pm 0.14) \times 10^{-4}. \quad (41)$$

We adopt a theoretical uncertainty of 7%, coming partly from non-perturbative effects [77, 118]. The corresponding likelihood has capability `b2sgamma_LL` (Table 8), and consists of a direct call to the standard `GAMBIT` Gaussian likelihood [4]. Note that in general the theoretical

calculation from `SuperIso` should be preferred over the corresponding quantity from `FeynHiggs` as input to this likelihood, as the cut employed on the photon energy in `SI_bsgamma` ($E_\gamma > 1.6$ GeV – see Table 2) is correctly matched to the cut applied in the experimental analysis.

The experimental correlation between $\mathcal{B}(B \rightarrow X_s\gamma)$ and the isospin asymmetry of $B \rightarrow K^*\gamma$ is not known, though it is expected to be non-negligible given that the event selections overlap. Because the inclusive branching ratio of $B \rightarrow X_s\gamma$ has a smaller theoretical uncertainty, we include $\mathcal{B}(B \rightarrow X_s\gamma)$ but not Δ_0 in the likelihood function.

5.5 B meson mass asymmetry likelihood

The parameters ΔM_s and ΔM_d have been precisely measured [91]:

$$\Delta M_d = 0.5064 \pm 0.0019 \text{ ps}^{-1}, \quad (42)$$

$$\Delta M_s = 17.757 \pm 0.021 \text{ ps}^{-1}. \quad (43)$$

The measurement of ΔM_d is the average of the results from the DELPHI, ALEPH, L3, OPAL, CDF, D0, BaBar, Belle and LHCb experiments, while the ΔM_s value is the average of the results from the CDF and LHCb experiments. The sensitivity of these observables is diluted by the theory uncertainty, which is essentially the same for both SM and BSM predictions, as it is dominated by lattice calculations of non-perturbative effects and the uncertainty on the B decay constant f_B . The total theoretical uncertainty on ΔM_s , for example, is currently 15% [119].

At present, `FlavBit` can predict only ΔM_s (Table 1), so the B meson mass asymmetry likelihood simply compares this prediction to Eq. 43, using a theoretical error of 15% and the standard `GAMBIT` Gaussian likelihood function [4]. This likelihood is available via the capability `deltaMB_LL` (Table 8).

5.6 Other observables

The $R_{\mu 23}$ average is dominated by the KLOE [120] and NA62 [121] experiments. While both R_μ and $R_{\mu 23}$ are implemented as observables in `FlavBit`, they are not included in the likelihood. For several BSM models, such as the 2HDM, they add negligible additional constraints, particularly when the decay $B^\pm \rightarrow \tau\nu_\tau$ is included in the likelihood via `SL_likelihood`.

6 Examples

Basic examples of how to use `FlavBit` in a `GAMBIT` BSM global fit can be found in any of the canonical `GAMBIT`

Parameter	Minimum	Maximum	Prior
m_0	50 GeV	7 TeV	log
$m_{\frac{1}{2}}$	50 GeV	5 TeV	log
A_0	-10 TeV	10 TeV	hybrid
$\tan \beta$	3	70	flat
$\alpha_s^{MS}(m_Z)$	0.1167	0.1203	flat
$m_{t,\text{pole}}$	171.06	175.62	flat

Table 9: CMSSM parameters varied in the example fit, along with their associated ranges and prior types. The “hybrid” prior on A_0 is logarithmic for $|A_0| > 100$ GeV and flat for $|A_0| < 100$ GeV.

SUSY examples in the `yaml_files` directory: `CMSSM.yaml`, `NUHM1.yaml`, `NUHM2.yaml` or `MSSM7.yaml` [4, 10, 11]. In this section, we go through a number of flavour-specific examples, ranging from flavour-only supersymmetric and effective field theory scans with GAMBIT, to an example of how to use FlavBit in standalone mode.

6.1 Supersymmetric scan

It is often instructive to consider the impacts of restricted classes of observables on broader global fits. In `yaml_files/FlavBit_CMSSM.yaml`, we give an example of a Constrained MSSM (CMSSM) fit focussing specifically on observables and likelihoods from FlavBit. This scan varies three dimensionful Lagrangian parameters defined at the GUT scale (the trilinear coupling A_0 , the universal scalar mass m_0 and the universal fermion mass $m_{\frac{1}{2}}$), the dimensionless ratio of Higgs VEVs at the weak scale ($\tan \beta$), and two SM nuisance parameters (α_s and m_t). The parameters and ranges are shown in Table 9.

In this example scan, we include the FlavBit rare leptonic and semileptonic (`SL_LL`), electroweak penguin (`b2s11_LL`), rare purely leptonic (`b211_LL`) and rare radiative likelihoods (`b2sgamma_LL`). In the interests of speed, numerical stability and comparability to the main CMSSM results presented in Ref. [10], we do not include the prediction of ΔM_s from FeynHiggs nor the resulting B mass asymmetry likelihood (`deltaMB_LL`). We employ nuisance likelihoods from PrecisionBit [14] to constrain α_s and m_t .

We focus specifically on the frequentist profile likelihood in this scan, and therefore employ differential evolution to sample the parameter space, as implemented in Diver [8]. Consistent with Ref. [10], we choose a population of 19200 and a convergence threshold of 10^{-5} . Although the profile likelihood is in principle independent of the chosen sampling method and prior, in practice these have an impact on the sampling efficiency and the ability of a scan to uncover more isolated likelihood

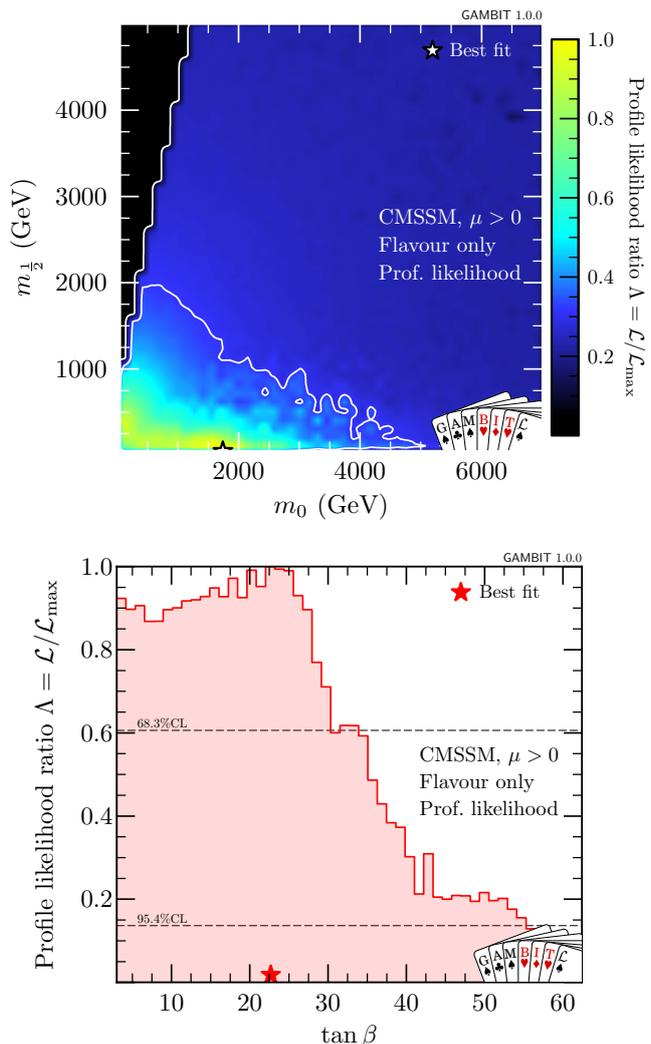


Fig. 1: 2D (upper) and 1D (lower) profile likelihoods of Lagrangian parameters m_0 , $m_{1/2}$ and $\tan \beta$ in a CMSSM fit including flavour and nuisance likelihoods only. Stars identify the best fit, and contours indicate 1 and 2σ confidence regions. The jagged edge of the 2σ contour at low m_0 and large $m_{1/2}$ is a plotting artefact, caused by interaction of the binning required for plotting and the abruptness of the dropoff of the likelihood in this region (due to the requirement that the lightest supersymmetric particle be a neutralino).

modes [8, 122, 123]. Our scans employ effectively logarithmic priors on the dimensionful BSM parameters, and flat priors on all other parameters. The SM parameters are sufficiently well constrained that the prior is irrelevant. We discuss the impact of the sampling prior on the BSM parameters below.

The resulting scan took approximately 15 minutes to run on 1200 CPU cores, and produced 1.1 million likelihood samples.

The results are shown in Fig. 1, in terms of the 2D profile likelihood of the sparticle masses m_0 and $m_{\frac{1}{2}}$,

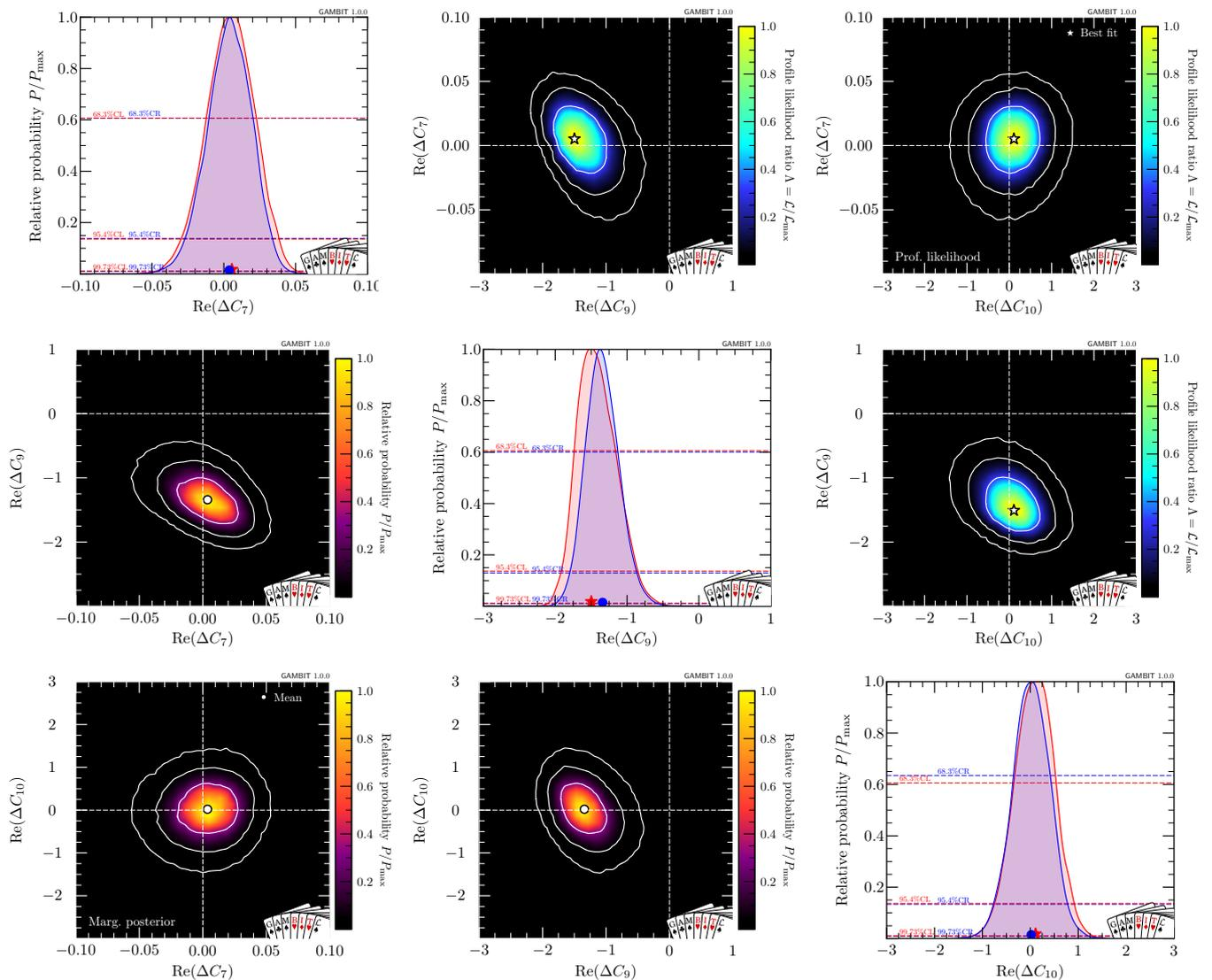


Fig. 2: Profile likelihoods (upper right panels) and posterior probabilities (bottom left panels) from a scan over the real parts of the Wilson coefficients C_7 , C_9 and C_{10} , expressed in terms of the offsets ΔC_i from the SM values. The central diagonal shows both 1D posterior probabilities (blue) and profile likelihoods (red) for each parameter. Stars indicate the location of the best fit, filled circles indicate posterior means, and contours correspond to 1, 2, and 3σ confidence. The SM prediction lies at the intersection of the dashed lines in the 2D panels.

and the 1D profile likelihood of $\tan\beta$. The flavour likelihoods have the most impact at large $\tan\beta$, as has been extensively pointed out in the literature (e.g. [72, 124]). The 2D figure shows a weak preference (at the 1–2 σ level) for lower sparticle masses. At first glance this may seem surprising, given the lack of hints for SUSY, the fact that the likelihood at large m_0 and $m_{\frac{1}{2}}$ essentially recovers the SM result, and the resulting tendency of $b \rightarrow s\gamma$ to drive SUSY fits to larger masses to avoid spoiling the good agreement between the SM prediction and the observed value of $\mathcal{B}(B \rightarrow X_s\gamma)$. Indeed, the likelihood improvement at low mass is driven entirely by the angular analysis of $B^0 \rightarrow K^*\mu^+\mu^-$ decays, with

the fit attempting to account for the deviation from the SM prediction in this channel by making the new states light and boosting the (generally small) SUSY contributions as much as possible. This effect is rather small, providing an improvement in the likelihood contribution from $B^0 \rightarrow K^*\mu^+\mu^-$ (`b2sll_likeliho`) of $\Delta\ln\mathcal{L} = 3.4$ relative to the SM. This improvement is mostly counteracted by a corresponding decrease of $\Delta\ln\mathcal{L} = -2.0$ in the likelihood associated with $\mathcal{B}(B \rightarrow X_s\gamma)$ (`b2sgamma_likeliho`).

6.2 Wilson coefficient fit

As a more advanced example, we carry out a joint fit to the real parts of the C_7 , C_9 and C_{10} effective couplings of Eq. 2, expressed in terms of offsets from their SM values $\Delta C_i \equiv C_i - C_{i,\text{SM}}$. The YAML file for this scan can be found at `yaml_files/WC.yaml`.

In this example, we use the electroweak penguin likelihood (`b2s11_likelihood`), the rare purely leptonic decay likelihood (`b211_likelihood`) and the rare radiative decay likelihood (`b2sgamma_likelihood`). The other two likelihood functions available in `FlavBit` (based on the B meson mass asymmetry and tree-level leptonic and semi-leptonic decays) have no dependence on the three Wilson coefficients that we vary. We also scan over the \overline{MS} b quark mass and the strong coupling as nuisance parameters, computing associated nuisance likelihoods with `PrecisionBit` [14]. We sample the parameter space with nested sampling [125, 126], using 20 000 live points and a tolerance of 0.1; see Ref. [8] for details of the scanning setup and sampling algorithm.

The results of this scan are shown in Fig 2. Here we show both Bayesian posterior probabilities (lower left panels) and frequentist profile likelihoods (upper right panels), which are in rather close agreement. The small offset between the peaks of the posterior and the profile likelihood in ΔC_9 is a volume effect, reflecting the fact that the posterior is slightly broader in C_7 and C_{10} at values below the best-fit ΔC_9 than above it. The results show a $> 3\sigma$ preference for a negative offset to the muonic version of the C_9 Wilson coefficient compared to the SM, consistent with recent results from other groups [127–129]. These are largely driven by the $B^0 \rightarrow K^* \mu^+ \mu^-$ angular observables, with the corresponding component of the best-fit likelihood improved by $\Delta \ln \mathcal{L} = 13.2$ with respect to the SM, and $\Delta \ln \mathcal{L} = 9.8$ compared to the CMSSM. We can also see that C_7 is strongly constrained by $b \rightarrow s\gamma$ decays, to within $+0.04/-0.03$ of its SM value.

6.3 FlavBit standalone example

GAMBIT modules can also be called directly from other codes as libraries, without actually needing to use GAMBIT itself. To do this, the calling code must specify the physics model and parameter set to be used, the module and backend functions to be run, and any required options. The calling code is responsible for resolving the dependencies and backend requirements of each module function; this is typically done “by hand” by the author of the calling code, using simple GAMBIT utility functions to hardcode the links between the chosen module and backend functions. More details of using GAMBIT

modules in this so-called ‘standalone mode’ can be found in Ref. [4].

An annotated driver program for calling `FlavBit` from outside the GAMBIT framework can be found in `FlavBit/examples/FlavBit_standalone_example.cpp`. As input, this program takes an SLHA file corresponding to the output of a spectrum generator (i.e. containing pole masses, \overline{DR} parameters, etc). The name of this file can be given as a command-line argument. The program then calculates the full menu of `FlavBit` observables using `SuperIso 3.6` and `FeynHiggs 2.11.3`, and uses them to calculate the five independent `FlavBit` likelihoods. Much of this short program is dedicated to resolving module function dependencies and backend requirements. This includes defining a local function that creates a `GAMBIT Spectrum` object from the input SLHA file, and others that fulfil the dependencies of `SI_fill` on the widths of the Z and W bosons.

If the user does not give the name of an input SLHA file when invoking the standalone example, it will read a default file given in the line

```
std::string infile("FlavBit/data/example.slha");
```

The likelihoods are retrieved in the lines

```
loglike = b211_likelihood(0);
loglike = b2s11_likelihood(0);
loglike = SL_likelihood(0);
loglike = b2sgamma_likelihood(0);
loglike = deltaMs_likelihood(0);
```

and can be combined or used for further analysis as the user requires.

The values of the observables, as used by the likelihoods, can be obtained directly from the respective observable functions in a similar manner, e.g.

```
double bsg = SI_bsgamma(0);
double Btaunu = SI_Btaunu(0);
```

and so on for all observables in Tables 1, 2 and 3.

7 Conclusions

In this paper we have described `FlavBit`, the flavour physics module of the public global-fitting framework GAMBIT. `FlavBit` provides calculations of a wide range of observables in flavour physics, ranging from tree-level decays of B and D mesons, to electroweak penguin decays, rare purely leptonic B decays, $b \rightarrow s\gamma$ transitions, neutral meson oscillations, kaon and pion decays, and various isospin and forward-backward asymmetries. These are so far implemented for supersymmetric and effective field theories, with the list of available theories expected to grow rapidly. `FlavBit` also features detailed

experimental data, uncertainties, correlations and likelihood functions for tree-level leptonic and semileptonic, electroweak penguin, rare purely leptonic and $B \rightarrow X_s \gamma$ decays, as well as for the $B_s^0 - \bar{B}_s^0$ mass difference.

We gave a number of interesting examples of FlavBit in action. These include a standalone example program that runs FlavBit without GAMBIT, in order to compute flavour observables in supersymmetry from an input SLHA file. We carried out an example supersymmetric flavour fit with FlavBit in GAMBIT, illustrating the impacts of its likelihoods. Finally, we performed a fit to a number of observables in the context of an effective theory of flavour, demonstrating about a 4σ preference from combined experimental data for an approximately 25% deficit in the (muonic) C_9 Wilson coefficient, compared to the Standard Model prediction.

The FlavBit source code can be freely downloaded from gambit.hepforge.org, either as part of GAMBIT, or as a standalone package.

Acknowledgements We thank our colleagues within GAMBIT for many helpful discussions. We warmly thank the Casa Matemáticas Oaxaca, affiliated with the Banff International Research Station, for hospitality whilst part of this work was completed, and the staff at Cyfronet, for their always helpful supercomputing support. GAMBIT has been supported by STFC (UK; ST/K00414X/1, ST/P000762/1), the Royal Society (UK; UF110191), Glasgow University (UK; Leadership Fellowship), the Research Council of Norway (FRIPRO 230546/F20), NOTUR (Norway; NN9284K), the Knut and Alice Wallenberg Foundation (Sweden; Wallenberg Academy Fellowship), the Swedish Research Council (621-2014-5772), the Australian Research Council (CE110001004, FT130100018, FT140100244, FT160100274), The University of Sydney (Australia; IRCA-G162448), PLGrid Infrastructure (Poland), Polish National Science Center (Sonata UMO-2015/17/D/ST2/03532), the Swiss National Science Foundation (PP00P2-144674), the European Commission Horizon 2020 Marie Skłodowska-Curie actions (H2020-MSCA-RISE-2015-691164), the ERA-CAN+ Twinning Program (EU & Canada), the Netherlands Organisation for Scientific Research (NWO-Vidi 680-47-532), the National Science Foundation (USA; DGE-1339067), the FRQNT (Québec) and NSERC/The Canadian Tri-Agencies Research Councils (BPDF-424460-2012).

Appendix A: Glossary

Here we explain some terms that have specific technical definitions in GAMBIT.

backend An external code containing useful functions (or variables) that one might wish to call (or read/write) from a **module function**.

backend function A function contained in a **backend**. It calculates a specific quantity indicated by its **capability**. Its capability and call signature are defined in the backend’s **frontend header**.

backend requirement A declaration that a given **module function** needs to be able to call a **backend function** or use a **backend variable**, identified according to its **capability** and type(s). Backend requirements are declared in module functions’ entries in **rollcall headers**.

backend variable A global variable contained in a **backend**. It corresponds to a specific quantity indicated by its **capability**. Its capability and type are defined in the backend’s **frontend header**.

capability A name describing the actual quantity that is calculated by a module or backend function. This is one possible place for units to be noted; the other is in the documented description of the capability (see Sec. 10.7 of Ref. [4]).

dependency A declaration that a given **module function** needs to be able to access the result of another module function, identified according to its **capability** and type. Dependencies are declared in module functions’ entries in **rollcall headers**.

dependency resolution The process by which GAMBIT determines the **module functions**, **backend functions** and **backend variables** needed and allowed for a given scan, connects them to each others’ **dependencies** and **backend requirements**, and determines the order in which they must be called.

frontend The interface between GAMBIT and a given **backend**, consisting of a **frontend header** plus optional source files and type headers.

frontend header The C++ header in which the **frontend** to a given **backend** is declared.

module A subset of GAMBIT functions following a common theme, able to be compiled into a standalone library. Although **module** often gets used as shorthand for **physics module**, this term technically also includes the GAMBIT scanning module ScannerBit.

module function A function contained in a **physics module**. It calculates a specific quantity indicated by its **capability** and **type**, as declared in the module’s **rollcall header**. It takes only one argument, by reference (the quantity to be calculated), and has a void return type.

physics module Any **module** other than ScannerBit, containing a collection of **module functions** following a common physics theme.

rollcall header The C++ header in which a given **physics module** and its **module functions** are declared.

type A general fundamental or derived C++ type, often referring to the type of the **capability** of a **module function**.

References

1. N. Serra, R. Silva Coutinho, and D. van Dyk, *Measuring the breaking of lepton flavor universality in $B \rightarrow K^* \ell^+ \ell^-$* , *Phys. Rev. D* **95** (2017) 035029, [[arXiv:1610.08761](#)].
2. D. Straub, *flav-io/flavio v0.20.3*, 2017. <https://doi.org/10.5281/zenodo.438351>.
3. e. L. Silvestrini, *HEPfit: a Code for the Combination of Indirect and Direct Constraints on High Energy Physics Models*, 2017. .
4. GAMBIT Collaboration: P. Athron, C. Balazs, et. al., *GAMBIT: The Global and Modular Beyond-the-Standard-Model Inference Tool*, *Eur. Phys. J. C in press* (2017) [[arXiv:1705.07908](#)].
5. F. Mahmoudi, *SuperIso: A Program for calculating the isospin asymmetry of $B \rightarrow K^* \gamma$ in the MSSM*, *Comp. Phys. Comm.* **178** (2008) 745, [[arXiv:0710.2067](#)].
6. F. Mahmoudi, *SuperIso v2.3: A Program for calculating flavor physics observables in Supersymmetry*, *Comp. Phys. Comm.* **180** (2009) 1579, [[arXiv:0808.3144](#)].
7. F. Mahmoudi, *SuperIso v3.0, flavor physics observables calculations: Extension to NMSSM*, *Comp. Phys. Comm.* **180** (2009) 1718.
8. GAMBIT Scanner Workgroup: G. D. Martinez, J. McKay, et. al., *Comparison of statistical sampling methods with ScannerBit, the GAMBIT scanning module*, *Eur. Phys. J. C in press* (2017) [[arXiv:1705.07959](#)].
9. GAMBIT Collaboration: P. Athron, C. Balázs, et. al., *Status of the scalar singlet dark matter model*, *Eur. Phys. J. C* **77** (2017) 568, [[arXiv:1705.07931](#)].
10. GAMBIT Collaboration: P. Athron, C. Balázs, et. al., *Global fits of GUT-scale SUSY models with GAMBIT*, *Eur. Phys. J. C in press* (2017) [[arXiv:1705.07935](#)].
11. GAMBIT Collaboration: P. Athron, C. Balázs, et. al., *A global fit of the MSSM with GAMBIT*, *Eur. Phys. J. C in press* (2017) [[arXiv:1705.07917](#)].
12. GAMBIT Collider Workgroup: C. Balázs, A. Buckley, et. al., *ColliderBit: a GAMBIT module for the calculation of high-energy collider observables and likelihoods*, *Eur. Phys. J. C in press* (2017) [[arXiv:1705.07919](#)].
13. GAMBIT Dark Matter Workgroup: T. Bringmann, J. Conrad, et. al., *DarkBit: A GAMBIT module for computing dark matter observables and likelihoods*, *Eur. Phys. J. C in press* (2017) [[arXiv:1705.07920](#)].
14. GAMBIT Models Workgroup: P. Athron, C. Balázs, et. al., *SpecBit, DecayBit and PrecisionBit: GAMBIT modules for computing mass spectra, particle decay rates and precision observables*, submitted to *Eur. Phys. J. C* (2017) [[arXiv:1705.07936](#)].
15. LHCb Collaboration: R. Aaij et. al., *Angular analysis and differential branching fraction of the decay $B_s^0 \rightarrow \phi \mu^+ \mu^-$* , *JHEP* **09** (2015) 179, [[arXiv:1506.08777](#)].
16. LHCb Collaboration: R. Aaij et. al., *Measurement of the ratio of branching fractions $\mathcal{B}(\bar{B}^0 \rightarrow D^{*+} \tau^- \bar{\nu}_\tau) / \mathcal{B}(\bar{B}^0 \rightarrow D^{*+} \mu^- \bar{\nu}_\mu)$* , *Phys. Rev. Lett.* **115** (2015) 111803, [[arXiv:1506.08614](#)]. [Addendum: *Phys. Rev. Lett.* **115**, no.15, 159901 (2015)].
17. LHCb Collaboration: R. Aaij et. al., *Test of lepton universality using $B^+ \rightarrow K^+ \ell^+ \ell^-$ decays*, *Phys. Rev. Lett.* **113** (2014) 151601, [[arXiv:1406.6482](#)].
18. LHCb Collaboration: R. Aaij et. al., *Measurement of Form-Factor-Independent Observables in the Decay $B^0 \rightarrow K^{*0} \mu^+ \mu^-$* , *Phys. Rev. Lett.* **111** (2013) 191801, [[arXiv:1308.1707](#)].
19. BaBar Collaboration: J. P. Lees et. al., *Evidence for an excess of $\bar{B} \rightarrow D^{(*)} \tau^- \bar{\nu}_\tau$ decays*, *Phys. Rev. Lett.* **109** (2012) 101802, [[arXiv:1205.5442](#)].
20. BaBar Collaboration: J. P. Lees et. al., *Measurement of an Excess of $\bar{B} \rightarrow D^{(*)} \tau^- \bar{\nu}_\tau$ Decays and Implications for Charged Higgs Bosons*, *Phys. Rev. D* **88** (2013) 072012, [[arXiv:1303.0571](#)].
21. Belle Collaboration: M. Huschle et. al., *Measurement of the branching ratio of $\bar{B} \rightarrow D^{(*)} \tau^- \bar{\nu}_\tau$ relative to $\bar{B} \rightarrow D^{(*)} \ell^- \bar{\nu}_\ell$ decays with hadronic tagging at Belle*, *Phys. Rev. D* **92** (2015) 072014, [[arXiv:1507.03233](#)].
22. Belle Collaboration: A. Abdesselam et. al., *Measurement of the branching ratio of $\bar{B}^0 \rightarrow D^{*+} \tau^- \bar{\nu}_\tau$ relative to $\bar{B}^0 \rightarrow D^{*+} \ell^- \bar{\nu}_\ell$ decays with a semileptonic tagging method*, [[arXiv:1603.06711](#)].
23. Belle Collaboration: A. Abdesselam et. al., *Angular analysis of $B^0 \rightarrow K^*(892)^0 \ell^+ \ell^-$* , in *Proceedings, LHCSki 2016 - A First Discussion of 13 TeV Results: Obergurgl, Austria, April 10-15, 2016* (2016) [[arXiv:1604.04042](#)].
24. M. Cacciari, G. P. Salam, and G. Soyez, *FastJet User Manual*, *Eur. Phys. J. C* **72** (2012) 1896, [[arXiv:1111.6097](#)].
25. P. Athron, J.-h. Park, D. Stöckinger, and A. Voigt, *FlexibleSUSY - A spectrum generator*

- generator for supersymmetric models, *Comp. Phys. Comm.* **190** (2015) 139–172, [[arXiv:1406.2319](#)].
26. B. C. Allanach, *SOFTSUSY: a program for calculating supersymmetric spectra*, *Comp. Phys. Comm.* **143** (2002) 305–331, [[hep-ph/0104145](#)].
 27. S. Heinemeyer, W. Hollik, and G. Weiglein, *FeynHiggs: A Program for the calculation of the masses of the neutral CP even Higgs bosons in the MSSM*, *Comp. Phys. Comm.* **124** (2000) 76–89, [[hep-ph/9812320](#)].
 28. Particle Data Group: C. Patrignani *et al.*, *Review of Particle Physics*, *Chin. Phys.* **C40** (2016) 100001.
 29. Y. Sakaki, M. Tanaka, A. Tayduganov, and R. Watanabe, *Testing leptoquark models in $\bar{B} \rightarrow D^{(*)}\tau\bar{\nu}$* , *Phys. Rev. D* **88** (2013) 094012, [[arXiv:1309.0301](#)].
 30. A. Crivellin, J. Heeck, and P. Stoffer, *A perturbed lepton-specific two-Higgs-doublet model facing experimental hints for physics beyond the Standard Model*, *Phys. Rev. Lett.* **116** (2016) 081801, [[arXiv:1507.07567](#)].
 31. M. Freytsis, Z. Ligeti, and J. T. Ruderman, *Flavor models for $\bar{B} \rightarrow D^{(*)}\tau\bar{\nu}$* , *Phys. Rev. D* **92** (2015) 054018, [[arXiv:1506.08896](#)].
 32. A. J. Buras and J. Girrbach, *Towards the Identification of New Physics through Quark Flavour Violating Processes*, *Rep. Prog. Phys.* **77** (2014) 086201, [[arXiv:1306.3775](#)].
 33. O. Eberhardt, U. Nierste, and M. Wiebusch, *Status of the two-Higgs-doublet model of type II*, *JHEP* **07** (2013) 118, [[arXiv:1305.1649](#)].
 34. D. Das, C. Hati, G. Kumar, and N. Mahajan, *Towards a unified explanation of $R_{D^{(*)}}$, R_K and $(g-2)_\mu$ anomalies in a L-R model*, [[arXiv:1605.06313](#)].
 35. A. Greljo, G. Isidori, and D. Marzocca, *On the breaking of Lepton Flavor Universality in B decays*, *JHEP* **07** (2015) 142, [[arXiv:1506.01705](#)].
 36. S. M. Boucenna, A. Celis, J. Fuentes-Martin, A. Vicente, and J. Virto, *Phenomenology of an $SU(2) \times SU(2) \times U(1)$ model with lepton-flavour non-universality*, [[arXiv:1608.01349](#)].
 37. D. Becirevic, N. Kosnik, O. Sumensari, and R. Zukanovich Funchal, *Palatable Leptoquark Scenarios for Lepton Flavor Violation in Exclusive $b \rightarrow s\ell_1\ell_2$ modes*, [[arXiv:1608.07583](#)].
 38. I. Dorsner, S. Fajfer, A. Greljo, J. F. Kamenik, and N. Kosnik, *Physics of leptoquarks in precision experiments and at particle colliders*, *Phys. Rep.* **641** (2016) 1–68, [[arXiv:1603.04993](#)].
 39. UTfit Collaboration: M. Bona *et al.*, *An Improved Standard Model Prediction Of $BR(B \rightarrow \tau\nu)$ And Its Implications For New Physics*, *Phys. Lett. B* **687** (2010) 61–69, [[arXiv:0908.3470](#)].
 40. A. G. Akeroyd and F. Mahmoudi, *Constraints on charged Higgs bosons from $D_{(s)}^\pm \rightarrow \mu^\pm\nu$ and $D_{(s)}^\pm \rightarrow \tau^\pm\nu$* , *JHEP* **04** (2009) 121, [[arXiv:0902.2393](#)].
 41. M. Beneke, T. Feldmann, and D. Seidel, *Systematic approach to exclusive $B \rightarrow V l^+ l^-$, $V\gamma$ decays*, *Nucl. Phys. B* **612** (2001) 25–58, [[hep-ph/0106067](#)].
 42. C. Greub, A. Ioannisian, and D. Wyler, *Effects of new physics in the rare decays $B \rightarrow K l^+ l^-$ and $B \rightarrow K^* l^+ l^-$* , *Phys. Lett. B* **346** (1995) 149–158, [[hep-ph/9408382](#)].
 43. F. Kruger and L. M. Sehgal, *Lepton polarization in the decays $b \rightarrow X_{(s)}\mu^+\mu^-$ and $B \rightarrow X_{(s)}\tau^+\tau^-$* , *Phys. Lett. B* **380** (1996) 199–204, [[hep-ph/9603237](#)].
 44. G. Hiller and F. Kruger, *More model independent analysis of $b \rightarrow s$ processes*, *Phys. Rev. D* **69** (2004) 074020, [[hep-ph/0310219](#)].
 45. LHCb Collaboration: R. Aaij *et al.*, *Differential branching fraction and angular analysis of the decay $B^0 \rightarrow K^{*0}\mu^+\mu^-$* , *JHEP* **08** (2013) 131, [[arXiv:1304.6325](#)].
 46. J. Gratx, M. Hopfer, and R. Zwicky, *Generalised helicity formalism, higher moments and the $B \rightarrow K_{J_K}(\rightarrow K\pi)\bar{\ell}_1\ell_2$ angular distributions*, *Phys. Rev. D* **93** (2016) 054008, [[arXiv:1506.03970](#)].
 47. LHCb Collaboration: R. Aaij *et al.*, *Angular analysis of the $B^0 \rightarrow K^{*0}\mu^+\mu^-$ decay using 3 fb^{-1} of integrated luminosity*, *JHEP* **02** (2016) 104, [[arXiv:1512.04442](#)].
 48. F. Beaujean, M. ChrzÄszcz, N. Serra, and D. van Dyk, *Extracting Angular Observables without a Likelihood and Applications to Rare Decays*, *Phys. Rev. D* **91** (2015) 114012, [[arXiv:1503.04100](#)].
 49. W. Altmannshofer, P. Ball, *et al.*, *Symmetries and Asymmetries of $B \rightarrow K^*\mu^+\mu^-$ Decays in the Standard Model and Beyond*, *JHEP* **01** (2009) 019, [[arXiv:0811.1214](#)].
 50. S. Descotes-Genon, T. Hurth, J. Matias, and J. Virto, *Optimizing the basis of $B \rightarrow K^*l$ observables in the full kinematic range*, *JHEP* **05** (2013) 137, [[arXiv:1303.5794](#)].
 51. F. Kruger and J. Matias, *Probing new physics via the transverse amplitudes of $B^0 \rightarrow K^{*0}(\rightarrow K^-\pi^+)l^+l^-$ at large recoil*, *Phys. Rev. D* **71** (2005) 094009, [[hep-ph/0502060](#)].
 52. D. Becirevic and E. Schneider, *On transverse asymmetries in $B \rightarrow K^*l^+l^-$* , *Nucl. Phys. B* **854** (2012) 321–339, [[arXiv:1106.3283](#)].

53. A. Bharucha, D. M. Straub, and R. Zwicky, *B* $\rightarrow V\ell^+\ell^-$ in the Standard Model from light-cone sum rules, *JHEP* **08** (2016) 098, [[arXiv:1503.05534](#)].
54. S. Jäger and J. Martin Camalich, *On B* $\rightarrow V\ell\ell$ at small dilepton invariant mass, power corrections, and new physics, *JHEP* **05** (2013) 043, [[arXiv:1212.2263](#)].
55. J. Lyon and R. Zwicky, *Resonances gone topsy turvy - the charm of QCD or new physics in b* $\rightarrow s\ell^+\ell^-$?, [[arXiv:1406.0566](#)].
56. M. Ciuchini, M. Fedele, *et. al.*, *B* $\rightarrow K^*\ell^+\ell^-$ decays at large recoil in the Standard Model: a theoretical reappraisal, *JHEP* **06** (2016) 116, [[arXiv:1512.07157](#)].
57. V. G. Chobanova, T. Hurth, F. Mahmoudi, D. Martinez Santos, and S. Neshatpour, *Large hadronic power corrections or new physics in the rare decay B* $\rightarrow K^*\mu^+\mu^-$?, *JHEP* **07** (2017) 025, [[arXiv:1702.02234](#)].
58. S. Descotes-Genon, J. Matias, and J. Virto, *Understanding the B* $\rightarrow K^*\mu^+\mu^-$ Anomaly, *Phys. Rev. D* **88** (2013) 074002, [[arXiv:1307.5683](#)].
59. W. Altmannshofer and D. M. Straub, *New physics in B* $\rightarrow K^*\mu\mu$?, *Eur. Phys. J. C* **73** (2013) 2646, [[arXiv:1308.1501](#)].
60. T. Hurth and F. Mahmoudi, *On the LHCb anomaly in B* $\rightarrow K^*\ell^+\ell^-$, *JHEP* **04** (2014) 097, [[arXiv:1312.5267](#)].
61. S. Jäger and J. Martin Camalich, *Reassessing the discovery potential of the B* $\rightarrow K^*\ell^+\ell^-$ decays in the large-recoil region: SM challenges and BSM opportunities, *Phys. Rev. D* **93** (2016) 014028, [[arXiv:1412.3183](#)].
62. T. Hurth, F. Mahmoudi, and S. Neshatpour, *On the anomalies in the latest LHCb data*, *Nucl. Phys. B* **909** (2016) 737–777, [[arXiv:1603.00865](#)].
63. LHCb Collaboration: R. Aaij *et. al.*, *Angular analysis of the B*⁰ $\rightarrow K^{*0}e^+e^-$ decay in the low- q^2 region, *JHEP* **04** (2015) 064, [[arXiv:1501.03038](#)].
64. T. Feldmann and J. Matias, *Forward-backward and isospin asymmetry for B* $\rightarrow K^*\ell^+\ell^-$ decay in the standard model and in supersymmetry, *JHEP* **1** (2003) 074, [[hep-ph/0212158](#)].
65. T. Huber, T. Hurth, and E. Lunghi, *Inclusive B* $\rightarrow X_s\ell^+\ell^-$: complete angular analysis and a thorough study of collinear photons, *JHEP* **06** (2015) 176, [[arXiv:1503.04849](#)].
66. BaBar Collaboration: B. Aubert *et. al.*, *Measurement of the B* $\rightarrow X_s\ell^+\ell^-$ branching fraction with a sum over exclusive modes, *Phys. Rev. Lett.* **93** (2004) 081802, [[hep-ex/0404006](#)].
67. Belle Collaboration: M. Iwasaki *et. al.*, *Improved measurement of the electroweak penguin process B* $\rightarrow X_s\ell^+\ell^-$, *Phys. Rev. D* **72** (2005) 092005, [[hep-ex/0503044](#)].
68. Belle Collaboration: Y. Sato *et. al.*, *Measurement of the lepton forward-backward asymmetry in B* $\rightarrow X_s\ell^+\ell^-$ decays with a sum of exclusive modes, *Phys. Rev. D* **93** (2016) 032008, [[arXiv:1402.7134](#)]. [Addendum: *Phys. Rev. D* **93**, no.5, 059901 (2016)].
69. BaBar Collaboration: J. P. Lees *et. al.*, *Measurement of the B* $\rightarrow X_sl^+\ell^-$ branching fraction and search for direct CP violation from a sum of exclusive final states, *Phys. Rev. Lett.* **112** (2014) 211802, [[arXiv:1312.5364](#)].
70. LHCb Collaboration: R. Aaij *et. al.*, *Differential branching fraction and angular moments analysis of the decay B*⁰ $\rightarrow K^+\pi^-\mu^+\mu^-$ in the $K_{0,2}^*(1430)^0$ region, *JHEP* **12** (2016) 065, [[arXiv:1609.04736](#)].
71. D. Das, G. Hiller, M. Jung, and A. Shires, *The B* $\rightarrow \bar{K}\pi\ell\ell$ and $\bar{B}_s \rightarrow \bar{K}K\ell\ell$ distributions at low hadronic recoil, *JHEP* **09** (2014) 109, [[arXiv:1406.6681](#)].
72. F. Mahmoudi, S. Neshatpour, and J. Virto, *B* $\rightarrow K^*\mu^+\mu^-$ optimised observables in the MSSM, *Eur. Phys. J. C* **74** (2014) 2927, [[arXiv:1401.2145](#)].
73. S. Bertolini, F. Borzumati, A. Masiero, and G. Ridolfi, *Effects of supergravity induced electroweak breaking on rare B decays and mixings*, *Nucl. Phys.* **B353** (1991) 591–649.
74. M. Misiak *et. al.*, *Estimate of B*($\bar{B} \rightarrow X_s\gamma$) at $O(\alpha_s^2)$, *Phys. Rev. Lett.* **98** (2007) 022002, [[hep-ph/0609232](#)].
75. F. Mahmoudi and O. Stål, *Flavor constraints on the two-Higgs-doublet model with general Yukawa couplings*, *Phys. Rev. D* **81** (2010) 035016, [[arXiv:0907.1791](#)].
76. T. Hermann, M. Misiak, and M. Steinhauser, *B* $\rightarrow X_s\gamma$ in the Two Higgs Doublet Model up to Next-to-Next-to-Leading Order in QCD, *JHEP* **11** (2012) 036, [[arXiv:1208.2788](#)].
77. M. Misiak *et. al.*, *Updated NNLO QCD predictions for the weak radiative B-meson decays*, *Phys. Rev. Lett.* **114** (2015) 221801, [[arXiv:1503.01789](#)].
78. M. Misiak and M. Steinhauser, *Weak Radiative Decays of the B Meson and Bounds on M_{H \pm} in the Two-Higgs-Doublet Model*, *Eur. Phys. J. C* **77** (2017) 201, [[arXiv:1702.04571](#)].
79. A. L. Kagan and M. Neubert, *QCD anatomy of B* $\rightarrow X(s\text{ gamma})$ decays, *Eur. Phys. J. C* **7** (1999) 5–27, [[hep-ph/9805303](#)].

80. A. L. Kagan and M. Neubert, *Isospin breaking in $B \rightarrow K^* \gamma$ decays*, *Phys. Lett.* **B539** (2002) 227–234, [[hep-ph/0110078](#)].
81. M. R. Ahmady and F. Mahmoudi, *Constraints on the $mSUGRA$ parameter space from NLO calculation of isospin asymmetry in $B \rightarrow K^* \gamma$* , *Phys. Rev. D* **75** (2007) 015007, [[hep-ph/0608212](#)].
82. M. González-Alonso and J. Martin Camalich, *Global Effective-Field-Theory analysis of New-Physics effects in (semi)leptonic kaon decays*, *JHEP* **12** (2016) 052, [[arXiv:1605.07114](#)].
83. FlaviaNet Working Group on Kaon Decays: M. Antonelli *et. al.*, *Precision tests of the Standard Model with leptonic and semileptonic kaon decays*, in *PHIPSI08, proceedings of the International Workshop on e^+e^- Collisions from phi to psi, Frascati (Rome) Italy, 7-10 April 2008* (2008) [[arXiv:0801.1817](#)].
84. A. J. Buras, P. H. Chankowski, J. Rosiek, and L. Slawianowska, $\Delta M_{d,s}$, $B^0 d, s \rightarrow \mu^+ \mu^-$ and $B \rightarrow X_s \gamma$ in supersymmetry at large $\tan \beta$, *Nucl. Phys.* **B659** (2003) 3, [[hep-ph/0210145](#)].
85. BaBar Collaboration: B. Aubert *et. al.*, *A Measurement of the branching fractions of exclusive $\bar{B} \rightarrow D^{(*)} (\pi) \ell^- \bar{\nu} (\ell)$ decays in events with a fully reconstructed B meson*, *Phys. Rev. Lett.* **100** (2008) 151802, [[arXiv:0712.3503](#)].
86. BaBar Collaboration: B. Aubert *et. al.*, *Measurement of $|V(cb)|$ and the Form-Factor Slope in anti- $B \rightarrow D \ell$ anti- ν Decays in Events Tagged by a Fully Reconstructed B Meson*, *Phys. Rev. Lett.* **104** (2010) 011802, [[arXiv:0904.4063](#)].
87. Belle Collaboration: W. Dungen *et. al.*, *Measurement of the form factors of the decay $B^0 \rightarrow D^{*+} \ell^+ \nu$ and determination of the CKM matrix element $|V_{cb}|$* , *Phys. Rev. D* **82** (2010) 112007, [[arXiv:1010.5620](#)].
88. Belle Collaboration: R. Glattauer *et. al.*, *Measurement of the decay $B \rightarrow D \ell \nu_\ell$ in fully reconstructed events and determination of the Cabibbo-Kobayashi-Maskawa matrix element $|V_{cb}|$* , *Phys. Rev. D* **93** (2016) 032006, [[arXiv:1510.03657](#)].
89. Belle Collaboration: Y. Sato *et. al.*, *Measurement of the branching ratio of $\bar{B}^0 \rightarrow D^{*+} \tau^- \bar{\nu}_\tau$ relative to $\bar{B}^0 \rightarrow D^{*+} \ell^- \bar{\nu}_\ell$ decays with a semileptonic tagging method*, *Phys. Rev. D* **94** (2016) 072007, [[arXiv:1607.07923](#)].
90. Belle Collaboration: S. Hirose *et. al.*, *Measurement of the τ lepton polarization and $R(D^*)$ in the decay $\bar{B} \rightarrow D^* \tau^- \bar{\nu}_\tau$* , [[arXiv:1612.00529](#)].
91. Y. Amhis *et. al.*, *Averages of b -hadron, c -hadron, and τ -lepton properties as of summer 2016*, [[arXiv:1612.07233](#)].
92. Y. Amhis *et. al.*, *Average of $R(D)$ and $R(D^*)$ for Moriond EW 2017*, <http://www.slac.stanford.edu/xorg/hfag/semi/moriond17/RDRDs.html>.
93. HPQCD Collaboration: H. Na, C. M. Bouchard, G. P. Lepage, C. Monahan, and J. Shigemitsu, *$B \rightarrow D \ell \nu$ form factors at nonzero recoil and extraction of $|V_{cb}|$* , *Phys. Rev. D* **92** (2015) 054510, [[arXiv:1505.03925](#)]. [Erratum: *Phys. Rev. D* **93**, no.11, 119906 (2016)].
94. S. Fajfer, J. F. Kamenik, and I. Nisandzic, *On the $B \rightarrow D^* \tau \bar{\nu}_\tau$ Sensitivity to New Physics*, *Phys. Rev. D* **85** (2012) 094025, [[arXiv:1203.2654](#)].
95. S. Fajfer, J. F. Kamenik, and I. Nišandžić, *$b \rightarrow D^* \tau \bar{\nu}_\tau$* , *Phys. Rev. D* **85** (2012) 094025.
96. Fermilab Lattice, MILC: J. A. Bailey *et. al.*, *$|V_{ub}|$ from $B \rightarrow \pi \ell \nu$ decays and $(2+1)$ -flavor lattice QCD*, *Phys. Rev. D* **92** (2015) 014024, [[arXiv:1503.07839](#)].
97. BaBar Collaboration: J. P. Lees *et. al.*, *Evidence of $B^+ \rightarrow \tau^+ \nu$ decays with hadronic B tags*, *Phys. Rev. D* **88** (2013) 031102, [[arXiv:1207.0698](#)].
98. BaBar Collaboration: B. Aubert *et. al.*, *A Search for $B^+ \rightarrow \ell^+ \nu_\ell$ Recoiling Against $B^- \rightarrow D^0 \ell^- \bar{\nu} X$* , *Phys. Rev. D* **81** (2010) 051101, [[arXiv:0912.2453](#)].
99. Belle Collaboration: I. Adachi *et. al.*, *Evidence for $B^- \rightarrow \tau^- \bar{\nu}_\tau$ with a Hadronic Tagging Method Using the Full Data Sample of Belle*, *Phys. Rev. Lett.* **110** (2013) 131801, [[arXiv:1208.4678](#)].
100. Belle Collaboration: K. Hara *et. al.*, *Evidence for $B^- \rightarrow \tau^- \bar{\nu}$ with a Semileptonic Tagging Method*, *Phys. Rev. D* **82** (2010) 071101, [[arXiv:1006.4201](#)].
101. ATLAS Collaboration, *Angular analysis of $B_d^0 \rightarrow K^* \mu^+ \mu^-$ decays in pp collisions at $\sqrt{s} = 8$ TeV with the ATLAS detector*, in *52nd Rencontres de Moriond on Electroweak Interactions and Unified Theories* (2017) ATLAS-CONF-2017-023.
102. CMS Collaboration, *Measurement of the P_1 and P'_5 angular parameters of the decay $B^0 \rightarrow K^{*0} \mu^+ \mu^-$ in proton-proton collisions at $\sqrt{s} = 8$ TeV*, in *52nd Rencontres de Moriond on Electroweak Interactions and Unified Theories* (2017) CMS-PAS-BPH-15-008.
103. F. Mahmoudi, T. Hurth, and S. Neshatpour, *Present Status of $b \rightarrow sl^+ l^-$ Anomalies*, in *6th Workshop on Theory, Phenomenology and Experiments in Flavour Physics: Interplay of Flavour Physics with electroweak symmetry breaking (Capri 2016) Anacapri, Capri, Italy*,

- June 11, 2016 (2016) [[arXiv:1611.05060](#)].
104. LHCb Collaboration: R. Aaij *et al.*, *Measurement of the $B_s^0 \rightarrow \mu^+ \mu^-$ branching fraction and effective lifetime and search for $B^0 \rightarrow \mu^+ \mu^-$ decays*, [arXiv:1703.05747](#).
 105. LHCb & CMS Collaborations: V. Khachatryan *et al.*, *Observation of the rare $B_s^0 \rightarrow \mu^+ \mu^-$ decay from the combined analysis of CMS and LHCb data*, *Nature* **522** (2015) 68–72, [[arXiv:1411.4413](#)].
 106. LHCb Collaboration: R. Aaij *et al.*, *Measurement of the $B_s^0 \rightarrow \mu^+ \mu^-$ branching fraction and search for $B^0 \rightarrow \mu^+ \mu^-$ decays at the LHCb experiment*, *Phys. Rev. Lett.* **111** (2013) 101805, [[arXiv:1307.5024](#)].
 107. CMS Collaboration: S. Chatrchyan *et al.*, *Measurement of the $B_s^0 \rightarrow \mu^+ \mu^-$ branching fraction and search for $B^0 \rightarrow \mu^+ \mu^-$ with the CMS Experiment*, *Phys. Rev. Lett.* **111** (2013) 101804, [[arXiv:1307.5025](#)].
 108. ATLAS Collaboration: M. Aaboud *et al.*, *Study of the rare decays of B_s^0 and B^0 into muon pairs from data collected during the LHC Run 1 with the ATLAS detector*, [arXiv:1604.04263](#).
 109. CDF Collaboration: T. Aaltonen *et al.*, *Search for the Decays $B_s^0 \rightarrow e^+ \mu^-$ and $B_s^0 \rightarrow e^+ e^-$ in CDF Run II*, *Phys. Rev. Lett.* **102** (2009) 201801, [[arXiv:0901.3803](#)].
 110. LHCb Collaboration: R. Aaij *et al.*, *Search for the decays $B_s^0 \rightarrow \tau^+ \tau^-$ and $B^0 \rightarrow \tau^+ \tau^-$* , [arXiv:1703.02508](#).
 111. BaBar Collaboration: B. Aubert *et al.*, *A search for the rare decay $B^0 \rightarrow \tau^+ \tau^-$ at BABAR*, *Phys. Rev. Lett.* **96** (2006) 241802, [[hep-ex/0511015](#)].
 112. A. J. Buras, J. Girrbach, D. Guadagnoli, and G. Isidori, *On the Standard Model prediction for $BR(B_{s,d} \rightarrow \mu^+ \mu^-)$* , *Eur. Phys. J. C* **72** (2012) 2172, [[arXiv:1208.0934](#)].
 113. BaBar Collaboration: B. Aubert *et al.*, *Measurement of the $B \rightarrow X_s \gamma$ branching fraction and photon energy spectrum using the recoil method*, *Phys. Rev. D* **77** (2008) 051103, [[arXiv:0711.4889](#)].
 114. BaBar Collaboration: J. P. Lees *et al.*, *Exclusive Measurements of $b \rightarrow s \gamma$ Transition Rate and Photon Energy Spectrum*, *Phys. Rev. D* **86** (2012) 052012, [[arXiv:1207.2520](#)].
 115. BaBar Collaboration: J. P. Lees *et al.*, *Precision Measurement of the $B \rightarrow X_s \gamma$ Photon Energy Spectrum, Branching Fraction, and Direct CP Asymmetry $A_{CP}(B \rightarrow X_{s+d} \gamma)$* , *Phys. Rev. Lett.* **109** (2012) 191801, [[arXiv:1207.2690](#)].
 116. Belle Collaboration: T. Saito *et al.*, *Measurement of the $\bar{B} \rightarrow X_s \gamma$ Branching Fraction with a Sum of Exclusive Decays*, *Phys. Rev. D* **91** (2015) 052004, [[arXiv:1411.7198](#)].
 117. Belle Collaboration: A. Abdesselam *et al.*, *Measurement of the inclusive $B \rightarrow X_{s+d} \gamma$ branching fraction, photon energy spectrum and HQE parameters*, in *Proceedings, 38th International Conference on High Energy Physics (ICHEP 2016): Chicago, IL, USA, August 3-10, 2016* (2016) [[arXiv:1608.02344](#)].
 118. M. Czakon, P. Fiedler, *et al.*, *The $(Q_7, Q_{1,2})$ contribution to $\bar{B} \rightarrow X_s \gamma$ at $\mathcal{O}(\alpha_s^2)$* , *JHEP* **04** (2015) 168, [[arXiv:1503.01791](#)].
 119. M. Artuso, G. Borissov, and A. Lenz, *CP violation in the B_s^0 system*, *Rev. Mod. Phys.* **88** (2016) 045002, [[arXiv:1511.09466](#)].
 120. KLOE Collaboration: F. Ambrosino *et al.*, *Precise measurement of $\Gamma(K \rightarrow e \nu(\gamma))/\Gamma(K \rightarrow \mu \nu(\gamma))$ and study of $K \rightarrow e \nu \gamma$* , *Eur. Phys. J. C* **64** (2009) 627–636, [[arXiv:0907.3594](#)]. [Erratum: *Eur. Phys. J. C* **65**, 703 (2010)].
 121. NA62 Collaboration: C. Lazzeroni *et al.*, *Precision Measurement of the Ratio of the Charged Kaon Leptonic Decay Rates*, *Phys. Lett. B* **719** (2013) 326–336, [[arXiv:1212.4012](#)].
 122. Y. Akrami, P. Scott, J. Edsjö, J. Conrad, and L. Bergström, *A profile likelihood analysis of the Constrained MSSM with genetic algorithms*, *JHEP* **4** (2010) 57, [[arXiv:0910.3950](#)].
 123. F. Feroz, K. Cranmer, M. Hobson, R. Ruiz de Austri, and R. Trotta, *Challenges of profile likelihood evaluation in multi-dimensional SUSY scans*, *JHEP* **6** (2011) 42, [[arXiv:1101.3296](#)].
 124. A. Arbey, M. Battaglia, F. Mahmoudi, and D. Martinez Santos, *Supersymmetry confronts $B_s \rightarrow \mu^+ \mu^-$: Present and future status*, *Phys. Rev. D* **87** (2013) 035026, [[arXiv:1212.4887](#)].
 125. J. Skilling, *Nested Sampling*, in *American Institute of Physics Conference Series* (R. Fischer, R. Preuss, and U. V. Toussaint, eds.) **735** (2004) 395–405.
 126. F. Feroz, M. P. Hobson, and M. Bridges, *MULTINEST: an efficient and robust Bayesian inference tool for cosmology and particle physics*, *MNRAS* **398** (2009) 1601–1614, [[arXiv:0809.3437](#)].
 127. T. Hurth, F. Mahmoudi, and S. Neshatpour, *Global fits to $b \rightarrow s \ell \ell$ data and signs for lepton non-universality*, *JHEP* **12** (2014) 053, [[arXiv:1410.4545](#)].

-
128. W. Altmannshofer, C. Niehoff, P. Stangl, and D. M. Straub, *Status of the $B \rightarrow K^* \mu^+ \mu^-$ anomaly after Moriond 2017*, [arXiv:1703.09189](#).
129. S. Descotes-Genon, L. Hofer, J. Matias, and J. Virto, *Global analysis of $b \rightarrow s \ell \ell$ anomalies*, *JHEP* **06** (2016) 092, [[arXiv:1510.04239](#)].